Check for updates

JGR Space Physics

RESEARCH ARTICLE
10.1029/2025JA033740

Special Collection:
Io and the Galilean Satellites

Modeling Jovian Plasma-Europa Interactions: Innovative Atmosphere and Ionosphere Depiction for JUICE Mission Insights

C. Baskevitch[1,2], R. Modolo[1], B. Cecconi[2], F. Leblanc[1], J.-E. Wahlund[3], S. Aizawa[4], and A. Oza[5]

[1]LATMOS/IPSL, UVSQ Université Paris-Saclay, Sorbonne Université, CNRS, Paris, France, [2]LIRA, Observatoire de Paris, Université PSL, CNRS, Sorbonne Université, Université de Paris Meudon, Paris, France, [3]Swedish Institute of Space Physics, Uppsala, Sweden, [4]LPP, Ecole polytechnique, Sorbonne Université, Institut Polytechnique de Paris, CNRS, Palaiseau, France, [5]Jet Propulsion Laboratory, California Institute of Technology, Pasadena, CA, USA

Key Points:

- A 3D hybrid model is used to simulate Europa's interactions with the jovian plasma during the Galileo E4 flyby and the future JUICE's flybys
- Three neutral/ionospheric environment models were compared, in order to observe the system's response to their variations
- An attempt for a realistic coupling between a 3D exosphere model and 3D kinetic plasma description of Europa-Jovian plasma interaction

Correspondence to:
C. Baskevitch,
claire.baskevitch@latmos.ipsl.fr

Citation:
Baskevitch, C., Modolo, R., Cecconi, B., Leblanc, F., Wahlund, J.-E., Aizawa, S., & Oza, A. (2025). Modeling jovian plasma-Europa interactions: Innovative atmosphere and ionosphere depiction for JUICE mission insights. *Journal of Geophysical Research: Space Physics*, *130*, e2025JA033740. https://doi.org/10.1029/2025JA033740

Received 13 JAN 2025
Accepted 29 OCT 2025

Abstract The JUpiter ICy moons Explorer (JUICE) mission, launched by the European Space Agency (ESA) in April 2023, aims to explore Jupiter and its icy moons, particularly focusing on Europa, Ganymede, and Callisto. This study uses the Latmos Hybrid Simulation (LatHyS) model to simulate Europa's plasma and field environment, emphasizing the upcoming JUICE flybys in July 2032. The LatHyS model, incorporating a detailed 3D exospheric model and a self-consistent ionosphere, allows for comprehensive analysis of the moon-plasma interactions at ion scales. Our simulations, validated against Galileo's E4 flyby data, demonstrate the model's accuracy in reproducing key features of the plasma environment and ionospheric dynamics. To characterize the system's response to neutral/ionospheric environment assumptions, we compare three simulations, with different neutral and ionosphere impacts, revealing the ionosphere's influence on the magnetic field intensity. Using an atmosphere derived from a planetary exosphere simulation model like EGM allows for the consideration of various asymmetries and multiple major neutral species, supporting further studies on ionospheric ion dynamics. Results highlight the complex interactions influenced by Europa's neutral and ionospheric conditions, providing insights for the anticipated JUICE observations. The measured signatures primarily depend on the interactions with the ionosphere along the spacecraft's trajectory and simulations show that a dense ionosphere deduced from radio occultation observations cannot reproduce the observed in situ signatures. The exosphere being a source for planetary ions, it was shown that it is significant to consider the spatial asymmetries in global interaction models in order to better account for its impact on the system.

Plain Language Summary The European Space Agency's JUpiter ICy moons Explorer (JUICE) mission, launched in April 2023, is set to explore Jupiter's icy moons Europa, Ganymede and Callisto. Two close flybys of Europa are scheduled in July 2032. JUICE will investigate in particular the moon's atmosphere, ionosphere, and its interactions with Jupiter's magnetosphere. To prepare for these observations, we used a computational model to simulate Europa's environment. In this model, we defined the atmosphere using two different methods. The first is to describe it analytically with a spherical symmetry assumption, which is the usual method. We have also chosen to introduce an atmosphere resulting from a model that allows us to introduce different species and asymmetries. By comparing these simulations with data from the Galileo mission, we confirm that the model effectively captures Europa's complex environment. The results suggest that the ionosphere has a significant effect on the size and properties of the induced planetary plasma cavity. We also conducted simulations for the upcoming JUICE mission flybys of Europa. These findings will help ensuring that the JUICE mission gathers meaningful data, enhancing our understanding of this intriguing moon and to better constrain the properties of a subsurface ocean.

© 2025. The Author(s).
This is an open access article under the terms of the Creative Commons Attribution-NonCommercial License, which permits use, distribution and reproduction in any medium, provided the original work is properly cited and is not used for commercial purposes.

1. Introduction

1.1. Overview of Europa's Environment

Europa orbits around Jupiter at 9.4 Jovian radii in the equatorial plane. Located within the region encompassing the outer edge of Io's torus and the inner magnetosphere of Jupiter, Europa experiences a magnetospheric field that exhibits quasi-dipolar characteristics. As a result of Jupiter's magnetic dipole axis being tilted by 9.6° relative to its rotational axis, the magnetic equator undergoes a sweeping motion over Europa. This sweeping occurs at a

21699402, 2025, 11, Downloaded from https://agupubs.onlinelibrary.wiley.com/doi/10.1029/2025JA033740 by Uppsala Universitet, Wiley Online Library on [04/12/2025]. See the Terms and Conditions (https://onlinelibrary.wiley.com/terms-and-conditions) on Wiley Online Library for rules of use; OA articles are governed by the applicable Creative Commons License

synodic period of 11.23 hr with respect to Europa, causing the magnetic equator to move up and down over the moon (Kivelson et al., 2004). The primary supplier of the plasma in the inner magnetosphere is Io, with O^+ and S^{++} being the primary ions resulting from the ionization and dissociation of Io's atmosphere and torus. Although Europa does contribute to the magnetospheric plasma supply, its contribution is relatively minor (Bagenal & Dols, 2020). The magnetospheric plasma corotates with Jupiter's angular velocity, and it overtakes the moon from its trailing hemisphere, at a velocity of approximately 100 km s^{-1} relative to Europa (Bagenal & Dols, 2020; Bagenal et al., 2015; Kivelson et al., 2009). This means that the plasma and magnetic field conditions of Europa vary periodically with Jupiter's rotation.

At Europa's orbit the background magnetic field is about 450 nT (Bagenal et al., 2015; Kivelson et al., 2009). The temporal variation of the ambient magnetic field induces an electric current in a conductive layer in the moon interior (Kivelson et al., 2000). Zimmer et al. (2000) and Kivelson et al. (2000) showed that a subsurface salty ocean at a depth of a few 100 km could generate a sufficient conductivity to produce the induction response observed by Galileo which creates an induced magnetic field. The recent study of Howell (2021) estimate the thickness of the icy shell to be about 23–47 km. The magnetospheric plasma, flowing at a sub-Alfvénic and subsonic velocity (u), undergoes deceleration as it interacts with the moon, but without forming a shock. The flow perturbation leads to the curvature of the magnetic field, propagating away from the moon in both directions toward Jupiter's ionosphere and along the field lines at the Alfvén speed (V_A), carried by an Alfvén wave. The perturbed region resulting from this interaction is commonly referred to as the Alfvén wings (Neubauer, 1980, 1998, 1999). A flow divergence is observed not only near the conducting moon but also around the Alfvén wings, characterized by a kink angle $\theta_A = \tan^{-1}(u/V_A)$ between the two Alfvén wings viewed in the moon rest frame (Kivelson et al., 2004; Neubauer, 1999).

Europa's atmosphere is a mixture of oxygen, water, and water-derived products, such as H_2, which are generated through surface sputtering and sublimation processes (Bagenal & Dols, 2020; Cassidy et al., 2013; Oza et al., 2018). Molecular oxygen (O_2) is expected to be the dominant component due to its unique properties that prevent it from freezing onto the surface like H_2O and escaping Europa's gravity as efficiently as H_2 (Johnson et al., 2009). Bagenal and Dols (2020) reported that the column density of O_2 in the atmosphere ranges from 2 to 15×10^{14} cm^{-2}. The existence of an atmosphere has been supported by the observation of UV auroras in atomic oxygen lines, as shown by Cassini UVIS observations during its Jupiter flyby (Hansen et al., 2005) and HST observations in UV (Roth et al., 2014, 2016). The detection of a tenuous ionosphere through radio occultation measurements (Kliore et al., 1997) supports the existence of a substantial atmosphere. The atmosphere of Europa may exhibit temporal and spatial variations, influenced by factors such as time-varying relative orientations of solar illumination and the incident plasma direction (Oza et al., 2018, 2019; Plainaki et al., 2013). Roth et al. (2014) and Sparks et al. (2016) discovered an additional source of neutrals originating from local and sporadic outgassing activity, water plumes, triggered by tidal effects that stress Europa's surface. Their localized occurrence have been observed primarily in the southern hemisphere. By adding a plume, Europa-jovian magnetosphere interaction models were also able to reproduce the magnetic signatures measured by Galileo, particularly during flybys E26 (Arnold et al., 2019; Blöcker et al., 2016) and E12 (Jia et al., 2018). Indirect evidence of plumes has also been observed through the examination of the ionosphere by Galileo radio occultation (McGrath & Sparks, 2017). High-density measurements by radio occultation coincide with repeated plume detection location observed by the Hubble Space Telescope (reported by Roth et al. (2014) and Sparks et al. (2016)). These asymmetries, not well constrained, can lead to density distribution variations among the different atmospheric species and induce asymmetries in the ionosphere.

Throughout this manuscript, the term ”ionosphere” will be used to describe the plasma population originated from the ionization of the neutral environment of the object, that creates a relatively dense and cold plasma region with respect to the upstream plasma property. The tenuous ionosphere of Europa mainly consists of O_2^+ ions, which are primarily produced through electron impact ionization from magnetospheric electrons, with a dominant rate of approximately 10^{-6} s^{-1} (Rubin et al., 2015; Saur et al., 1998; Schilling et al., 2008). Photoionization also contributes, but to a second order, with an estimated rate of a few 10^{-8} s^{-1} (Saur et al., 1998). However, it is important to note that the contribution of photoionization might become significant near the subsolar point, and especially in regions where electron impact ionization is weak, such as near the surface in the wake regions or when the ambient magnetospheric plasma density is low. The ionosphere were analyzed during six radio occultations of Europa conducted by the Galileo spacecraft between 1996 and 1997 (Kliore et al., 1997) and two radio

occultations during the Juno's E45 flyby on 29 September 2022 (Parisi et al., 2023). The findings show notable day/night and flanks/wake asymmetries with a decrease in electron density observed on the night and wake sides. Parisi et al. (2023) noted that Juno's E45 egress and Galileo's E4 ingress, which have similar geometry (5° latitude and 25° longitude difference) but different conditions (Night/Flanks vs. Day/Flanks), show plasma extending to high altitudes with a similar electron density of approximately 5,000 cm^{-3}. However, the authors pointed that it seems challenging to consider this observation as evidence of a dependence from geographic location, as there are currently not enough radio occultation observations. Kliore et al. (1997) reported an average electron density scale height of 240 ± 40 km below 300 km with an electron density peak of approximately 9,000 cm^{-3} close to the surface. As for Juno's observations, Parisi et al. (2023) reported a smaller electron density peak between 4,000 and 6,000 cm^{-3} confined to low altitudes with an overall scale height of 405 ± 205 km. In addition, a localized plume-ionosphere were reported to explain the prominent magnetic signatures on the Galileo E12 (Jia et al., 2018) and E26 (Arnold et al., 2019; Blöcker et al., 2016) flybys, associated to a sharp peak in electron density near the closest approach. This implies that the ionosphere's composition could also change, with H_2O^+ potentially becoming the dominant ion in plume regions and near the subsolar point. Furthermore, electron beams were detected during the Juno E45 flyby, which are associated with large jumps of the magnetic field, and locally enhance ionization (Allegrini et al., 2024). The ionosphere of Europa is thus likely to be asymmetric and inhomogeneous due to the influence of electron flow patterns and the potentially inhomogeneous atmosphere. Ionospheric particles experience a downstream transport by plasma particles, ultimately accelerating to co-rotation speeds and resulting in the development of a narrow plasma wake. A thorough description of Europa's ionosphere is critical to better understand the moon-magnetosphere interaction. This entails examining the three-dimensional distribution of ionospheric densities and composition, as well as their response to solar, magnetospheric, and orbital conditions.

1.2. Summary of Plasma Interaction Models

In the past 25 years, significant progress has been made in understanding the interaction between the Jovian magnetosphere and Europa's atmosphere/ionosphere. Various MHD and hybrid models have been developed to explore different aspects of this interaction.

Saur et al. (1998) employed a three-dimensional MHD model to investigate the interaction between the Jovian magnetosphere and Europa's atmosphere/ionosphere, identifying the main sources and sinks that maintain the neutral atmosphere. They determined that electron impact ionization was the primary process contributing to the generation of new ions. Saur et al. (1998) derived an oxygen column density of 5×10^{18} m^{-2}, in agreement with the radiative output in atomic oxygen line emission observed by the Hubble Space Telescope. This column density provided further support for the balance between production and loss processes that regulate the overall composition of Europa's atmosphere.

Kabin et al. (1999) and Liu et al. (2000) investigated the Europa-Magnetosphere interactions during the Galileo E4 flyby. Kabin et al. (1999) used a single-fluid MHD model, while Liu et al. (2000) presented a two-fluid model representing magnetospheric ions and ionospheric O_2^+. Kabin et al. (1999) demonstrated the necessity of including an induced magnetic field in the model to reproduce the measured magnetic signatures from the Galileo mission, supporting the results presented by Zimmer et al. (2000) and Kivelson et al. (2000). Liu et al. (2000) provided more precise estimations of plasma flows and the impact of the ionosphere on electromagnetic interactions through their two-species model.

Schilling et al. (2007, 2008) used a single-fluid MHD model to examine the influence of the induced magnetic field on the plasma environment surrounding Europa. Schilling et al. (2007) established a relationship between the thickness of the ocean and its electrical conductivity to explain the observed magnetic field data. Schilling et al. (2008) demonstrated that the induced magnetic field modifies the current and plasma density, leading to asymmetric structure of the plasma flow in the wake. This asymmetry explains the absence of high ionospheric plasma densities convected downstream during the Galileo E4 flyby.

Lipatov et al. (2010, 2013) developed a multi-species hybrid model to study the effects of the different possible magnetospheric composition. The hybrid model enabled accurate estimation of velocity distributions and considered the kinetic effects of the interactions. The authors revealed time-dependent structures in the pick-up

21699402, 2025, 11, Downloaded from https://agupubs.onlinelibrary.wiley.com/doi/10.1029/2025JA033740 by Uppsala Universitet, Wiley Online Library on [04/12/2025]. See the Terms and Conditions (https://onlinelibrary.wiley.com/terms-and-conditions) on Wiley Online Library for rules of use; OA articles are governed by the applicable Creative Commons License

ion tails within the plasma wake, analog to the plasma wake observed in comets. Moreover, ion and electron temperatures were identified as important factors influencing plasma structure formation.

Rubin et al. (2015) presented a 3D multi-fluid MHD model accounting for the complex interplay between the neutral atmosphere and the plasma populations originating from Jupiter's magnetosphere and Europa's ionosphere. To accurately represent the characteristics of Europa's atmosphere, the authors incorporated an asymmetry between the upstream and downstream regions. In their model, one fluid was dedicated to representing O^+ ions, encompassing both the thermal magnetospheric ions and the cold ionospheric O^+ ions generated from the atmosphere. Additionally, a second fluid was employed to specifically represent the cold ionospheric O_2^+. By incorporating a diverse range of source and loss terms, the model effectively captured the intricate dynamics and interactions between the plasma and the atmosphere. Rubin et al. (2015) successfully computed separate production and loss rates for each fluid, taking into account not only mass but also the momentum and pressure associated with the two ion populations.

In their recent work, Harris et al. (2021) expanded upon the model developed by Rubin et al. (2015) by introducing a three-ion-fluid MHD model. The authors employed distinct fluids to represent the magnetospheric O^+, and the two ionospheric species O_2^+ and O^+ ions produced by the atmosphere. Their objective was to investigate the influence of variations of the external magnetospheric plasma on Europa's environment and to analyze the precipitation rate of magnetospheric plasma at Europa under different magnetospheric conditions. They reported that the precipitation rate increased with higher densities of magnetospheric plasma, primarily due to the ionization of the atmosphere through electron impacts. Harris et al. (2022) further explored the effects of Europa's atmosphere on the overall properties of the plasma and magnetic fields in Europa's plasma interaction. They observed that increasing the column density of the atmosphere led to a corresponding increase in the column density of the ionosphere and of the pile up of magnetic field upstream of the moon. Consequently, simulations with higher atmospheric column densities exhibited reduced precipitation of magnetospheric plasma.

Recent research has focused on investigating the effects of water plumes on the environment near Europa. Blöcker et al. (2016) employed a MHD model to demonstrate that atmospheric inhomogeneities have an impact on the plasma environment, magnetic field, and Alfvén wings, resulting in a north/south asymmetry. They further suggested that the magnetic field perturbations observed during the Galileo E26 flyby could be attributed to a plume in the southern hemisphere. This hypothesis was supported by Arnold et al. (2019), using a hybrid model. Building upon this work, Arnold, Liuzzo, and Simon (2020) examined the influence of atmospheric inhomogeneities on the plasma interaction between Europa and Jupiter's magnetosphere. Furthermore, Jia et al. (2018) incorporated a plume into the Rubin et al. (2015) model and successfully demonstrated that it could account for the magnetic signatures observed during the Galileo E12 flyby.

1.3. Future Mission of Exploration

The JUpiter ICy moons Explorer (JUICE) mission, launched on 14 April 2023, will represent a significant advancement in the study of the system of Jupiter and its icy moons. This European Space Agency (ESA) L-class mission is equipped with three instrument packages designed to investigate in situ particles and fields. These instruments and consortium of instruments include the magnetometer (J-MAG) (Dougherty, 2025), the particle environment package (PEP) (Barabash, 2025), and the Radio and Plasma Wave Investigation (RPWI) instrument (Wahlund et al., 2025). The primary objectives of the mission consist in the characterization of the three largest icy moons of Jupiter, Europa, Ganymede, and Callisto, as well as studying their exospheres, ionospheres, and potential outgassing activity in case of Europa. In this study, we focus on Europa and we consider the configuration that JUICE might encounter during its two flybys. Based on the kernels proposed by the ESA Space Operation Center (SOC) and their reference trajectory CReMA 5.1, the first flyby (7E1) will occur on 2 July 2032, and the second on 16 July 2032, with closest approaches at an altitude of about 401 km. These flybys will take place near the north and south poles of Europa, respectively, and on the anti-jovian hemisphere. The second flyby (8E2) of the JUICE mission is of great significance since it will take place in the southern hemisphere where previous observations have revealed outgassing activity, and will occur quasi-simultaneously with the Europa Clipper mission of NASA, with a few hours of difference, marking the first time that two missions will explore a moon of Jupiter in a multi-points perspective, thereby will offer a unique opportunity to improve the characterization of the plasma dynamic and the electromagnetic field behavior in Europa's ionized environment.

21699402, 2025, 11, Downloaded from https://agupubs.onlinelibrary.wiley.com/doi/10.1029/2025JA033740 by Uppsala Universitet, Wiley Online Library on [04/12/2025]. See the Terms and Conditions (https://onlinelibrary.wiley.com/terms-and-conditions) on Wiley Online Library for rules of use; OA articles are governed by the applicable Creative Commons License

21699402, 2025, 11, Downloaded from https://agupubs.onlinelibrary.wiley.com/doi/10.1029/2025JA033740 by Uppsala Universitet, Wiley Online Library on [04/12/2025]. See the Terms and Conditions (https://onlinelibrary.wiley.com/terms-and-conditions) on Wiley Online Library for rules of use; OA articles are governed by the applicable Creative Commons License

1.4. Outline

In this paper, we focus on the hybrid model LatHyS to study the plasma and field environment of Europa. First, we provide an overview of the model, including the coupling between a neutral exospheric model EGM (Oza et al., 2018, 2019) and the hybrid model. In Section 3, we present the environment parameters used for the study. In Section 4, we start by validating our approach by comparing the LatHyS model outputs with Galileo observations obtained during the E4 flyby. Then, we study how the system respond to different neutral and ionospheric environments and finally, we analyze the upcoming 7E1 and 8E2 flybys of JUICE.

2. Methods

In the past 30 years, global three-dimensional models have emerged as a powerful tool to investigate the complex planetary plasma environment. Among them, LatHyS (Latmos Hybrid Simulation) stands out as a model that combines a fluid description of electrons with a kinetic treatment of ions. This so called hybrid approach allows for a more comprehensive description of the phenomena occurring at the ion scale. While it is computationally more demanding than a fluid model, it relies on fewer assumptions and includes more physics (Hall term, Larmor radius effect, etc.). It also enables precise identification of the origins of ions with the same m/q ratio, whether from incident plasma, electron impact, photoionization, or other sources. LatHyS has been developed for various planetary environments such as Mars (Modolo et al., 2016), Mercury (Richer et al., 2012), Ganymede (Leclercq et al., 2016) and more recently Venus (Aizawa et al., 2022). Here, we aim to describe Europa's environment and improve the model by using a global exospheric model instead of the commonly used analytical description to reproduce the exosphere. In this section, we provide a brief overview of the LatHyS model and discuss the adaptations that were made to simulate Europa's plasma environment.

2.1. Model Description

Hybrid models enable the description of physical phenomena at ion scales providing information on kinetic features of the moon-plasma interaction, and are therefore complementary to MHD models. In these models, the electrons are treated as a fluid with no inertia, contributing to the electric current and maintaining the neutrality of the plasma, while kinetic description is adopted for the ions (Kallio et al., 2011; Ledvina et al., 2008). Following a Lagrangian perspective, LatHyS is a Hybrid Particle-In-Cell (PIC) code. In practice, the Vlasov equation governing the evolution of the distribution function for each ion population is not directly solved, but its solution can be obtained by the evolution of a collection of numerical particles called macroparticles. A macroparticle does not represent individual ions but a cloud of physical ions having the same physical properties. These macroparticles behave like physical particles and follow the laws governing the motion of physical particles.

$$\frac{d\mathbf{x}_p}{dt} = \mathbf{v}_p \tag{1}$$

$$m_p \frac{d\mathbf{v}_p}{dt} = q_p(\mathbf{E} + \mathbf{v}_p \times \mathbf{B} - \boldsymbol{\eta}\mathbf{J}) + \mathbf{F_c} \tag{2}$$

where, m_p and q_p are the mass and charge of the particle p and $\mathbf{x}_p$ and $\mathbf{v}_p$ are the position and velocity of the macroparticle respectively. $\boldsymbol{\eta}$ is a resistivity term and is defined in Equation 8. $\mathbf{F_c} = m_p \nu_{in}(\mathbf{u}_n - \mathbf{v}_p)$ is the drag force applied on the macroparticle, with $\mathbf{u}_n$ the velocity of the neutrals. We assume that the neutrals are at rest in the planetary frame and therefore have a velocity of zero. ν_{in} represents an average of the ion-neutral collision frequency for momentum transfer (Banks & Kockarts, 1973). It can be approximated by $\nu_{in} = 2.6 \times 10^{-9} n_n (\alpha_0/\mu_A)^{1/2}$ s^{-1} where n_n is the neutral number density in cm^{-3}, μ_A is the ion-neutral reduced mass in atomic units, and α_0 is the atomic polarizability ($\alpha_0 = 1.59 \times 10^{-24}$ cm^{-3} for O_2).

The density n_s of ion species "s" is determined from the distribution function

$$n_s(\mathbf{x}, t) = \int f_s(\mathbf{x}, \mathbf{v}, t) d^3v \tag{3}$$

21699402, 2025, 11, Downloaded from https://agupubs.onlinelibrary.wiley.com/doi/10.1029/2025JA033740 by Uppsala Universitet, Wiley Online Library on [04/12/2025]. See the Terms and Conditions (https://onlinelibrary.wiley.com/terms-and-conditions) on Wiley Online Library for rules of use; OA articles are governed by the applicable Creative Commons License

The bulk velocity and the ionic current of species "s" are therefore

$$\mathbf{u}_s(\mathbf{x},t) = \frac{1}{n_s(\mathbf{x},t)} \int \mathbf{v} f_s(\mathbf{x},\mathbf{v},t) d^3v \tag{4}$$

$$\mathbf{J_s}(\mathbf{x},t) = q_s n_s(\mathbf{x},t) \mathbf{u}_s(\mathbf{x},t) \tag{5}$$

In the hybrid formalism, the electric field is derived from the equation of conservation of the electron momentum. This approach relies on two main assumptions: the electrons are treated as a massless fluid, and a quasi-neutrality condition $\left(n_e = \sum_{s=ions} n_s\right)$ is maintained. Consequently, the resulting equation can be expressed in the form of Ohm's law. Considering the focus on low-frequency phenomena, the contribution of the displacement current term in Ampère's equation can be disregarded. As a result, the electric field can be computed as:

$$\mathbf{E} = \frac{1}{en_e}\left(\frac{\nabla \times \mathbf{B}}{\mu_0}\right) \times \mathbf{B} - \mathbf{u_i} \times \mathbf{B} - \frac{1}{en_e} \nabla P_e + \boldsymbol{\eta} \frac{\nabla \times \mathbf{B}}{\mu_0} \tag{6}$$

with n_e the electron number density, e the electron charge, $\mathbf{u_i}$ the ion velocity, P_e the electron pressure, μ_0 the vacuum magnetic permeability, $\mathbf{E}$ and $\mathbf{B}$ the electric and magnetic fields.

The pressure tensor, which we assume to be isotropic, serves as the closing equation of our system. It is expressed as follows:

$$\overline{\overline{\mathbf{P}}}_\mathbf{e} = n_e \gamma k_B T_e \overline{\overline{I}} \tag{7}$$

with k_B the Boltzmann constant, T_e the electronic temperature and γ the adiabatic index of the fluid.

The treatment of electrons in the model involves considering them as two separate fluids, each requiring a distinct closing equation. One fluid represents the incident plasma electrons, while the other represents the ionospheric electrons (Modolo & Chanteur, 2008). The behavior of the incident plasma electrons is assumed to be adiabatic ($\gamma = 5/3$), while the ionospheric electron population follows a polytropic equation with a varying index γ between 0 (isobaric process) and 5/3 (adiabatic process). This polytropic index is adjusted according to the electron density, facilitating a smooth transition from the deep ionospheric region (Modolo et al., 2016), where a barotropic ionosphere is assumed, to the upstream region where adiabatic behavior is expected. The inclusion of this varying polytropic index prevents the inward and outward effects of the electronic gradient pressure force below and above the ionospheric peak, respectively. As a result, it helps to reduce the diffusion and expansion of the ionospheric region.

The resistivity term, $\boldsymbol{\eta}$, represents the collisions of electrons with neutrals and ions. This term is included in Ohm's law (Equation 6) and in the equations of motion to provide the momentum balance.

$$\boldsymbol{\eta} = \frac{1}{\sigma_e} = \frac{1}{\sigma_{en}} + \frac{1}{\sigma_{ei}} \approx \frac{\nu_{en} m_e}{e^2 n_e} \tag{8}$$

with σ_e is the electron conductivity derived from the collision frequencies, ν_{en}, of the electron with neutrals and ions (cf. Section 2.6).

The model relies on the CAM-CL algorithm (Matthews, 1994), and Modolo et al. (2016) provide a comprehensive account of the numerical scheme. The authors specifically elaborate on aspects such as the parallelization and performance of the model, the spatial domain decomposition, the computation of the moments and fields, and the management of particles.

2.2. Neutral Atmosphere Description

In order to evaluate the influence of the ionospheric description on the global Europa-Jupiter interaction, the atmosphere of Europa has been described following two approaches. The first is to adopt an analytical approach based on empirical observation, the second is a new step toward a more realistic description with the

implementation of a 3D description of Europa's neutral environment as described by the "Exospheric Global Model" (Leblanc et al., 2017; Oza et al., 2018).

2.2.1. Case 1: Analytical Description

Europa's atmosphere consists of molecular oxygen, which is the dominant specie. We adopted the same atmospheric description than Harris et al. (2021), which is also similar to those used in previous models for Europa's plasma interaction (Rubin et al., 2015). The neutral atmosphere has a surface density of $n_0 = 2.5 \times 10^7$ cm^{-3} and a scale height of $H_0 = 100$ km, assuming a spherical symmetry profile:

$$n_{O_2}(z) = n_0 \exp(-z/H_0) \tag{9}$$

with z the altitude in km.

2.2.2. Case 2: Loading a 3D Neutral Environment From the EGM

"Exospheric Global Model" (EGM) is a Monte-Carlo model that simulates the creation and evolution of a planetary exosphere composed of several species (Leblanc et al., 2017; Oza et al., 2018). The coupling between LatHyS and EGM consists in loading the 3D exosphere calculated by EGM at initialization in the LatHyS model.

The simulation domain of EGM is defined by a non-uniform 3D spherical grid with coordinates in the system denoted as (r, θ, φ). The size of the radial component cells, r, increases with altitude. For example, in the case of Europa, the surface cell measures 1 km in altitude, while the last cell measures 100 km, allowing for a better description of regions near the surface. In longitude, the grid is uniformly divided, and in latitude, the grid is divided according to an arccosine function, ensuring each cell has the same surface area at a given altitude.

Macroscopic quantities (density, average velocity, and temperature) are calculated within the grid cells. In contrast, LatHyS calculates these quantities at the nodes of the Cartesian grid. The coupling between EGM results and LatHyS is done as follows:

- For each LatHyS grid node, an influence region of the node is defined, that is, the size of a LatHyS cell $(\Delta x, \Delta y, \Delta z)$ centered on the node.
- The density n_j^{LatHyS} of LatHyS node j is equal to the average of the density n_i^{EGM} of cells i in the EGM grid where at least a part of the cell is within the influence region of node j.

$$n_j^{LatHyS} = \frac{\sum n_i^{EGM} \times V_i^{EGM}}{\sum V_i^{EGM}} \tag{10}$$

where V_i^{EGM} is the volume of cell i in the EGM grid.

The accurate representation of the EGM atmosphere in LatHyS depends on the spatial resolution of the latter and the height scale of the neutral species. The closer LatHyS spatial resolution is to the height scale of the neutral species (or smaller), the better the density of the neutral species, and thus the ion production, will be described.

2.3. Ionization Sources

The neutral atmosphere of Europa serves as a source of new born ions, mainly by electron impact ionization from corotating (or nearly corotating) plasma and also by photoionization. Charge exchanges reactions between jovian or ionospheric ions with neutral environments are also implemented.

2.3.1. Electron Impact

Following the same approach than Rubin et al. (2015) and similarly to Cravens et al. (1987), the ionization rate is obtained by integrating the product of the normalized Maxwellian energy distribution of the electrons $f_e(E, T_e)$ at temperature T_e and electron impact ionization cross section $\sigma_X^e(E)$ of specie $X = O_2, H_2O, H_2$ taken from Hwang et al. (1996). The electron impact frequency is therefore given by

21699402, 2025, 11, Downloaded from https://agupubs.onlinelibrary.wiley.com/doi/10.1029/2025JA033740 by Uppsala Universitet, Wiley Online Library on [04/12/2025]. See the Terms and Conditions (https://onlinelibrary.wiley.com/terms-and-conditions) on Wiley Online Library for rules of use; OA articles are governed by the applicable Creative Commons License

21699402, 2025, 11, Downloaded from https://agupubs.onlinelibrary.wiley.com/doi/10.1029/2025JA033740 by Uppsala Universitet, Wiley Online Library on [04/12/2025]. See the Terms and Conditions (https://onlinelibrary.wiley.com/terms-and-conditions) on Wiley Online Library for rules of use; OA articles are governed by the applicable Creative Commons License

Table 1
Coefficients of the Polynomial Electron Impact Frequency Function (13) for Each Species

	a_1	a_2	a_3	a_4	a_5	$\nu^e_{X^+}$ $[s^{-1}]$ [a]
O_2	−352.134	88.1318	−8.882784	0.4082678	−0.0072026	$(0.8-3.9) \times 10^{-6}$
H_2O	−390.080	98.8605	−10.001035	0.4592265	−0.0080629	$(0.8-3.8) \times 10^{-6}$
H_2	−489.841	126.3080	−12.813012	0.5855403	−0.0101690	$(0.4-1.8) \times 10^{-6}$

[a]The last column indicates the electron impact ionization rates for two set of n_e, T_e jovian plasma parameters used for the Galileo and JUICE simulations respectively (Table 4).

$$\nu^e_{X^+}(T_e) = \int_{Q^{pot}_X}^{\infty} f_e(E,T_e)\sigma^e_X(E)v_e(E)dE \tag{11}$$

Only electrons possessing energies greater than the ionization potential, Q^{pot}_X, can ionize. This specifically concerns the incident electron population. The Maxwell-Boltzmann energy distribution at temperature T_e is

$$f_e(E,T_e) = 2\sqrt{E/\pi}\left(\frac{1}{kT_e}\right)^{3/2}\exp\left(\frac{-E}{kT_e}\right) \tag{12}$$

For simplicity we have fitted the electron impact frequency for $n_e = 1$ cm^{-3} in function of the electron temperature as a polynomial function

$$\nu^e_{X^+}(T_e) = \exp\left(\sum_{j=1,5} a_j\,(\ln(T_e))^{j-1}\right) \tag{13}$$

with a_j described in Table 1 for each specie $X = O_2, H_2O, H_2$ and Figure 1 gives the ionization frequency in function of the energy.

Therefore, the production by electron impact is computed locally according to the electron density and temperature, and the neutral density,

$$q^e_{X^+} = n_e\nu^e_{X^+}(T_e)\,n_X \tag{14}$$

with n_X the neutral density of species $X = O_2, H_2O, H_2$.

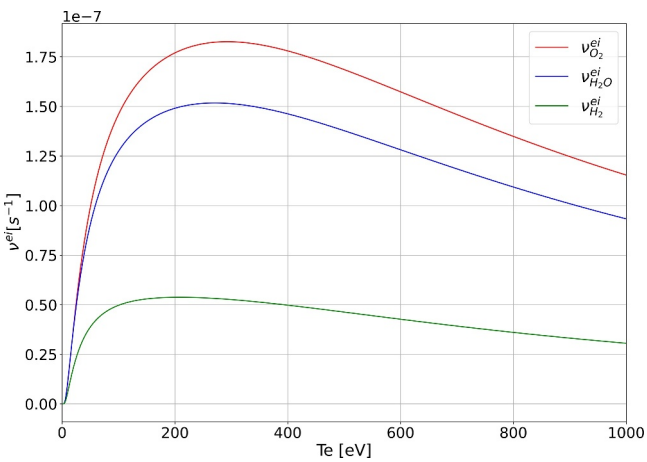

Figure 1. Electron impact ionization frequency in function of the energy of each species.

2.3.2. Photoionization

Photoproduction is determined using the Extreme UltraViolet flux model for Aeronomics Calculations (EUVAC) developed by Richards et al. (1994). EUVAC uses a reference spectrum consisting of 37 wavelength intervals ranging from 5 to 105 nm. Given the tenuous nature of Europa's atmosphere, the process of photoabsorption is disregarded. Photoionization occurs throughout the moon's atmosphere, excluding areas within its shadow. The calculation of production follows the standard expression as provided by Shunk and Nagy (2004):

$$q^{photo}_{X^+} = n_X\int_0^{\lambda_t}\sigma^{photo}_X I_\infty(\lambda)\exp[-\tau(Z,\lambda,\chi)]d\lambda \tag{15}$$

Here, $q^{photo}_{X^+}$ represents the production rate of ion species X^+, n_X denotes the neutral density of component X, and I_∞ represents the solar EUV flux without attenuation, calculated using the EUVAC model by Richards et al. (1994). For

21699402, 2025, 11, Downloaded from https://agupubs.onlinelibrary.wiley.com/doi/10.1029/2025JA033740 by Uppsala Universitet, Wiley Online Library on [04/12/2025]. See the Terms and Conditions (https://onlinelibrary.wiley.com/terms-and-conditions) on Wiley Online Library for rules of use; OA articles are governed by the applicable Creative Commons License

Table 2
Photoionization Frequencies Scaled to a Heliocentric Distance of 5.2 AU

Reaction	ν^{photo} (s^{-1})
$O_2 + h\nu \rightarrow O_2^+ + e^-$	1.7×10^{-8}
$H_2O + h\nu \rightarrow \begin{cases} H_2O^+ + e^- & + \\ OH^+ + H + e^- & + \\ O^+ + OH + e^- \end{cases}$	1.42×10^{-8}
$H_2 + h\nu \rightarrow H_2^+ + e^-$	2.0×10^{-9}

each species, the corresponding photoionization cross sections σ_X^{photo} were taken from the work of Schunk (2004). In the case of H_2O, the cross sections for the specific reactions specified in Table 2 were summed together, the products are considered to be W^+ water-group ions with a mass of 18 amu. The ionization rates of O_2^+ derived from this model align with the findings reported by Huebner et al. (1992) scaled to a heliocentric distance of about 5.2 AU.

2.4. Ionospheric Description

To accelerate the convergence of the simulation, we start the simulation with pre-defined ionospheric profiles, either based on an empirical profile derived from Galileo radio occultation measurements, or build from ionization reactions applied to a 3D atmosphere. Ionospheric macroparticles are loaded in the simulation from the surface up to 600 km according to the ionospheric profile at initialization.

During the simulation, ionospheric particles are free to move and we compute locally at each time step the local production that contributes to supply the ionospheric plasma. To ensure the stability during the transition phase to reach a stationary condition, 20% of initial ionospheric macroparticles below 600 km are frozen, and thus acts as a fluid background ionosphere.

2.4.1. Case 1: Analytical Description

In the case where the atmosphere is defined analytically, we define the ionosphere in the same way. Radio-occultation observations of Europa have been performed with the Galileo spacecraft, revealing the presence of a tenuous ionosphere. Kliore et al. (1997) derived an average electron density profile with a maximum electron density near 10^4 cm^{-3} close to the surface and a plasma scale height of 240 +/− 40 km from the surface to 300 km altitudes and of 440 +/− 60 km above 300 km. In our simulations, we use a surface density of 2500 cm^{-3} and two scale height: $H_0 = 240$ km from the surface to 300 km and $H_1 = 440$ km from 300 to 600 km.

2.4.2. Case 2: Consistent 3D Ionosphere From EGM

For this case, we build the ionosphere from the EGM exosphere profiles presented in Section 2.2.2. To ensure that the ionosphere represents the dynamics of the exosphere and each neutral population, we do not use an empirical profile. Instead, we calculate ion production from electron impact and photoionization over a period of time, assuming that the plasma environment, fields and particles are frozen. In our model, we don't consider recombination as a loss reaction, so we need to determine a satisfactory integration time of the ionosphere. To determine the integration time, we calculated the production of O_2^+ ions on the atmospheric profile presented in Section 2.2.1 until we reach the surface density of the empirical ionospheric profile presented in Section 2.4.1 of 2500 cm^{-3}. We reached this surface density with 10 gyroperiods of incident plasma O^+ and chose this value as the integration time for EGM exospheric ionization at initialization.

2.5. Charge Exchange

Charge exchange reactions occur when an incident ion X^+ collides with a neutral M, resulting in the production of an energetic neutral atom (ENA) and a cold ion M^+. As the model does not consider the dynamics of neutrals, the

Table 3
Charge Exchange Cross-Sections

Reaction	$\sigma_{X^+,M}^{CX}$ (cm^2)	Energy range	References
$O_{jv}^+ + O_2 \rightarrow O + O_2^+$	4.2×10^{-16}	250 eV	Lindsay & Stebbings (2005)
$O_{jv}^+ + H_2O \rightarrow O + H_2O^+$	25×10^{-16}	[0.5, 0.8] keV	Lindsay et al. (2001)
$O_{jv}^+ + H_2 \rightarrow O + H_2^+$	4.8×10^{-16}	<3 keV	Hoffman et al. (1982)
$O_2^+ + O_2 \rightarrow O_2 + O_2^+$	4.2×10^{-16}	250 eV	Lindsay & Stebbings (2005)

21699402, 2025, 11, Downloaded from https://agupubs.onlinelibrary.wiley.com/doi/10.1029/2025JA033740 by Uppsala Universitet, Wiley Online Library on [04/12/2025]. See the Terms and Conditions (https://onlinelibrary.wiley.com/terms-and-conditions) on Wiley Online Library for rules of use; OA articles are governed by the applicable Creative Commons License

Table 4
Simulation and Plasma Parameters for Galileo E4 Flyby and JUICE 7E1 and 8E2 Flybys

	Galileo E4	JUICE 7E1	JUICE 8E2
Closest approach (CA)	12/19/1996 06:52:58 UTC	07/02/2032 16:22:30 UTC	07/16/2032 22:18:00 UTC
Europa's Local Time (h)	16.8	16.0	19.0
S3 Lon. [°]	157	117	−40
CA [km]	688.1	401.6	401.3
CA (x,y,z) $[R_E]$	(0.84,1.17,0.03)	(0.005, −0.86, 0.92)	(−0.1, −1.06, −0.66)
(B_{Jx},B_{Jy},B_{Jz}) [nT]	(65, −173, −412)	(−71, −86, −460)	(36, 148, −460)
(M_x,M_y,M_z) [nT]	(−27, 88, 0)	(35.5,43,0)	(−18, −74, 0)
N_{O^+} [cm^{-3}]	20	100	100
$U_{O^+,x}$ [km s^{-1}]	100	100	100
T_e [eV]	20	20	20
T_i [eV]	129	130	130

Note. S3 Lon. is the position of Europa in Jupiter's System III, B_j is the jovian magnetic field, M is Europa's magnetic moment, N_{O^+} is the jovian O^+ density, $U_{O^+,x}$ is the jovian O^+ velocity, T_e and T_i are the electron and ion temperature of the plasma environment.

produced neutral is no longer included in the model and is treated as an outgoing particle. The model considers two types of incident ions: O^+ originating from the Jovian plasma and O_2^+ from the ionosphere. The effective cross-sections $\sigma^{CX}_{X^+,M}$ for each of the considered reactions are listed in Table 3.

The charge exchange ionization rate is calculated as:

$$q_M^{CX} = \sigma^{CX}_{X^+,M} n_M n_{X^+} u_{X^+} \tag{16}$$

where u_{X^+} represents the velocity of the incident ion, and n_M and n_{X^+} denote the densities of the neutral M and the ion X^+, respectively.

To determine if an ion will undergo a charge exchange reaction, we compute the collision probability for each incident macroparticle (O^+ or O_2^+) at each time step. The probability depends on factors such as the effective cross-section, the density of the neutral M, the speed of the incident particle, and the time step. The detailed explanation of the probability calculation can be found in the work by Modolo et al. (2016).

2.6. Electron-Neutral Collision and Resistivity

Schunk and Nagy (2009) defined the collision frequency of Equation 8 as:

$$\nu_{en} = 1.82 \times 10^{-10} n_n \left(1 + 3.6 \times 10^{-2} \sqrt{T_e}\right) \sqrt{T_e} \tag{17}$$

For simplification we assume a constant electron temperature of 20 eV, and we defined the resistivity by a linear function. The resistivity varies from 5.5×10^5 $\Omega.m$ at the surface to 10^4 $\Omega.m$ at 600 km.

3. Model Parameters and Initial and Boundary Conditions

3.1. Jovian Plasma Parameters

The plasma parameters used in our simulations are summarized in Table 4.

According to Kim et al. (2020), based on the Jovian Auroral Distributions Experiment Ion (JADE-I) onboard JUNO, in the equatorial region of Jupiter's magnetosphere, the most dominant ions species are O^+ and S^{++}. Since both ion species have the same mass-to-charge ratio, we consider the magnetospheric plasma made of O^+ ions

21699402, 2025, 11, Downloaded from https://agupubs.onlinelibrary.wiley.com/doi/10.1029/2025JA033740 by Uppsala Universitet, Wiley Online Library on [04/12/2025]. See the Terms and Conditions (https://onlinelibrary.wiley.com/terms-and-conditions) on Wiley Online Library for rules of use; OA articles are governed by the applicable Creative Commons License

only. Therefore, the underlying hypothesis is that charge exchange reactions between S^{++} and the neutral atmosphere constituents behave like reactions with O^{+} ions. For simulations corresponding to the plasma conditions observed during the Galileo E4 flyby we use the same jovian background magnetic field than Harris et al. (2021). It has been determined by linearly fitting the flyby magnetometer data, excluding the perturbed values within ≈ 10 min of closest approach, and selecting the linear fit magnetic field values at closest approach. For the representation of the induced magnetic field, we used the magnetic moment values for the E4 flyby as reported in Kivelson et al. (2000). The magnetic moment is given as a magnetic field vector with the equatorial strength of the magnetic field at Europa's surface. The upstream total ion density of 20 cm^{-3} and upstream velocity of 100 km s^{-1} for the E4 flyby are reported in Paterson et al. (1999).

For the JUICE flybys, the jovian background magnetic field is determined by the model of Connerney et al. (2018), derived from data collected by the Juno spacecraft, and we chose the value by using the same methodology as described in the previous paragraph. We calculated the magnetic moment of Europa's induced dipole assuming 100% efficient induction by the time-varying components of the magnetospheric magnetic field (B_{Jx} and B_{Jy}) such that $M_x[nT] = -B_{Jx}/2$ and $M_y[nT] = -B_{Jy}/2$ (Harris et al., 2021; Kivelson et al., 2000).

Jupiter's rotation axis is tilted by 10° relative to the magnetic dipole axis. Consequently, Jupiter's magnetosphere oscillates around Europa, leading to variations in electromagnetic fields and plasma properties. Jupiter's plasma sheet center is inclined by 7° relative to the moon's orbital plane (Bagenal et al., 2015). As Jupiter rotates and Europa approaches the plasma sheet center, the magnetospheric plasma tends to become colder and denser. Conversely, when Europa moves away from the plasma sheet center, the magnetospheric plasma becomes hotter and less dense. Plasma parameters are based on the models by Bagenal et al. (2015). The authors proposed three cases corresponding to the moon's relative position to the plasma sheet (low-density and high-temperature; medium-density and medium-temperature; high-density and cold-temperature). We chose the medium case and considered only the cold electron population. Bagenal et al. (2015) reported an average electron density of 100 cm^{-3} at the JUICE flybys' longitudes, an electron temperature of 20 eV, and an ion temperature of 130 eV.

3.2. Boundary and Initial Conditions

In our hybrid model, the plasma and magnetic field environment of Europa is represented by a three-dimensional uniform Cartesian grid with EphiO coordinates. Specifically, the X axis is along the plasma flow direction, the Y axis is along the Europa-Jupiter vector, and the Z axis is aligned with Jupiter's spin axis. The model assumes that the incident plasma is injected at the entry plane $X = -6.5R_E$, following a Maxwellian velocity distribution, and leaves the simulation domain at the exit plane $X = 6.5R_E$ with R_E the radius of Europa ($R_E = 1560$ km). We apply periodic boundary conditions in the Y and Z directions ($Y = [-15, 15]R_E$ and $Z = [-15, 15]R_E$) for particles and fields, while setting the velocity of a particle to zero when it hits the planetary body.

During the initialization process, every cell is initially filled with 10 macroparticles, representing the specified jovian plasma density for each run as indicated in Table 4. These macroparticles are assigned velocities following the Maxwellian distribution function. Subsequently, the ionosphere is populated with a specific number of particles based on the density and weight given to ionospheric macroparticles. At the start of the simulation, Jovian macroparticles are present in every cell of the simulation box. There is therefore a transition phase during which the exclusion cavity (Europa and the ionospheric region) is formed and excludes the Jovian macroparticles. In the simulation, this phase lasts 50 $\Omega_{O^+}^{-1}$. It prevents the unnecessary escape of ionospheric macroparticles by allowing sufficient time for the magnetospheric plasma to be slow down by the mass loading incorporated, diverted around the obstacle and draped around the moon. At the end of this transition phase, the constraint on ionospheric macroparticles is released, which then follow a natural $E \times B$ drift.

3.3. Atmosphere From "Exospheric Global Model"

Some models simulate an ionosphere constructed from an atmosphere modeled by the 3D Monte-Carlo EGM model (Beth et al., 2025; Carnielli et al., 2019; Werner et al., 2022). EGM reproduces the dynamics of Europa's neutral exosphere as the moon orbits Jupiter (Oza et al., 2019). The effects of Europa's rotation on the dusk/dawn asymmetry of O_2 and the asymmetry of H_2O on the day side are particularly apparent. Water molecules are produced by sublimation and sputtering of the icy surface, they follow a ballistic trajectory and then stick to the surface. The density is higher near the subsolar point. Radiolysis of water produces molecular oxygen and

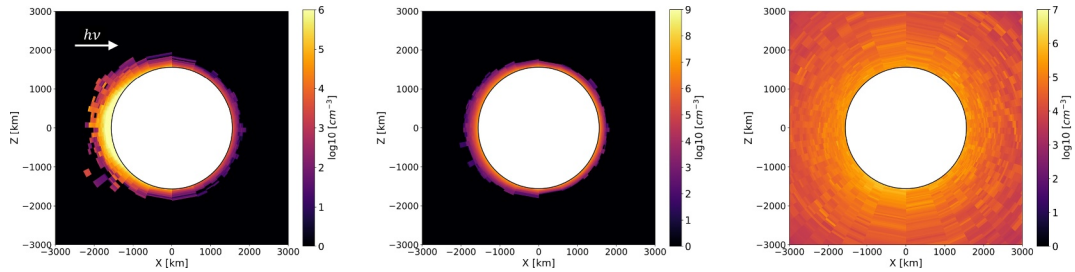

Figure 2. Density of Europa's exosphere, in EphiO coordinate system, simulated by EGM at LT 16:00 in the XZ plane. From left to right are the densities of H_2O, O_2 and H_2.

molecular hydrogen which then follow ballistic trajectory. O_2 is too heavy to escape the gravitational attraction of Europa and don't stick to the surface like water, becoming the most prominent specie in the atmosphere. H_2 is lighter and has a much larger height scale than the other two species, as they tend to escape Europa's gravitational attraction more easily. We therefore use the state of the exosphere at the different local times corresponding to the flybys. The local times are close, so there are few differences between the exospheres. Figure 2 shows the density for the three neutral species considered in the XZ plane.

4. Results

4.1. A Case Study on Galileo E4 Flyby

To demonstrate the validity of the simulation model, the conditions of the Galileo E4 flyby have been used in order to compare with observational data. The flyby occurred on 19 December 1996, with a closest approach (CA) of 688 km from the surface.

Three simulations, named A1, A2 and A3, were carried out (see Table 5), using the Jovian plasma parameters summarized in Table 4.

Simulations were performed over at least 60,000 time steps with a time step of $\Delta t = 0.01\Omega_{O^+}$. This corresponds to two complete transits through the simulation domain (along the X axis) for an unperturbed Jovian plasma particle. The simulation domain is cut by a uniform 3D cartesian grid with a spatial resolution of $\Delta x = 0.5c/\omega_{pi} = 100$ km. We used $200 \times 450 \times 450$ grid points and about 8×10^8 particles.

4.1.1. Global Results on Galileo E4 Flyby

In this section, we focus on the comparison between Galileo data and simulation results for RUN A1. The impact of the ionosphere/exosphere is discussed in Section 4.1.2.

We first depict the main characteristics of the interaction of the Jovian plasma with Europa using simulation RUN A1. When a magnetized plasma flows toward a conductive obstacle like a moon with an ionosphere, it slows down and is diverted around the moon where the velocity streamlines are compressed on the flanks causing the plasma to be accelerated up to 300 km s^{-1}. The disturbance of the magnetic field, created by this interaction and referred as the Alfvén wings, can be observed extending from north to south. The plasma and the Jovian ambient magnetic field cannot penetrate the conductive ionosphere due to currents. The O^+ ions are accumulated upstream of Europa until they reach about 100 cm^{-3} (Figure 3).

Figure 4 presents the equatorial (XY), XZ, and YZ planes of the density of ionospheric O_2^+ ions. Galileo's probe followed a trajectory in the equatorial plane and passed through the moon's wake. Its trajectory is plotted in black on the figure. On the ionospheric density plots, an escape of the ionosphere toward the wake is observed on the pro-Jovian side (Figure 4a) and along the Alfvén wings (Figures 4b and 4c). In the MHD simulations of Rubin et al. (2015) and Harris et al. (2021), the wake is located in the region of the geometric wake (toward $Y = 0$ and $Z = 0$) because fluid simulations do not

Table 5
Parameters of the Different Simulations

	RUN A1	RUN A2	RUN A3
Plasma parameters	Galileo E4	Galileo E4	Galileo E4
Exosphere model	Analytical	Analytical	EGM
ionosphere model	Analytical	Self-consistent	Self-consistent

Note. Refer to Table 4 for the plasma parameters of each flybys. The Analytical descriptions for atmosphere/ionosphere are described in Sections 2.2.1 and 2.4.1. The EGM model used for the neutral environment is described in Section 2.2.2 and the self-consistent ionosphere is detailed in Section 2.4.2.

21699402, 2025, 11, Downloaded from https://agupubs.onlinelibrary.wiley.com/doi/10.1029/2025JA033740 by Uppsala Universitet, Wiley Online Library on [04/12/2025]. See the Terms and Conditions (https://onlinelibrary.wiley.com/terms-and-conditions) on Wiley Online Library for rules of use; OA articles are governed by the applicable Creative Commons License

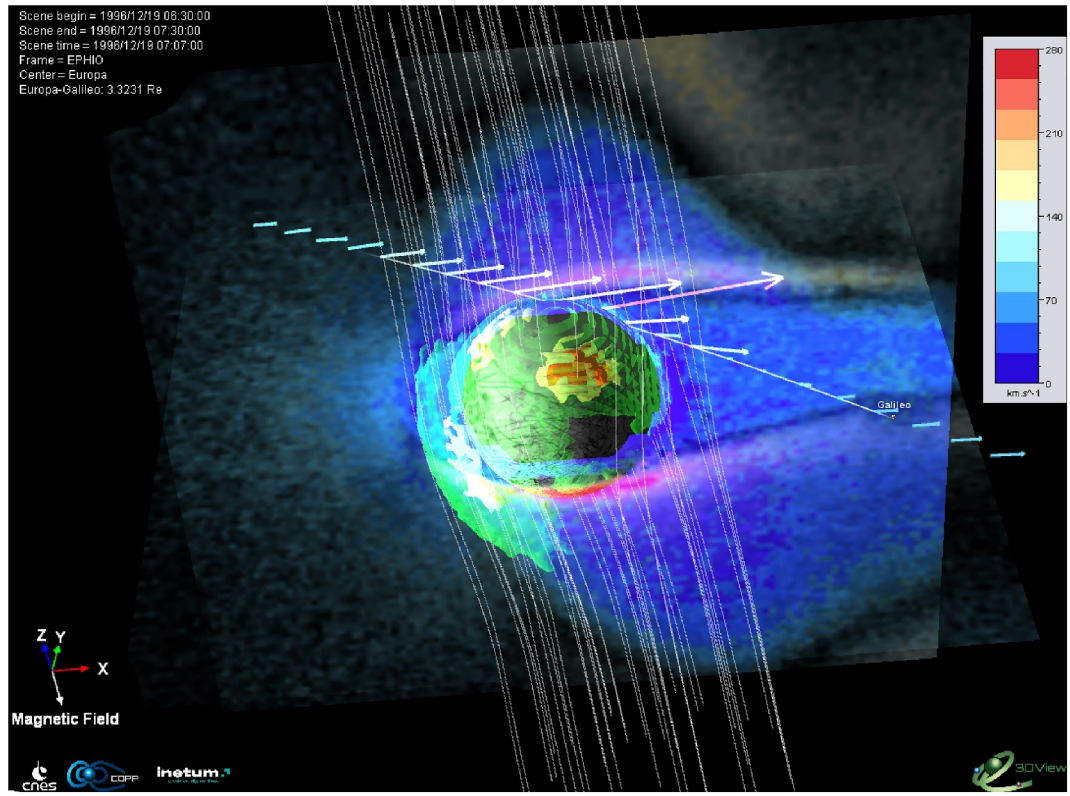

Figure 3. 3D figure showing Europa's interactions with the Jovian plasma, simulated with configuration RUN A1 and using 3D View software. Magnetic field lines are in white, and the density of the Jovian O^+ ions is given by iso-contours: green $n_{O^+} > 50$ cm^{-3}, yellow $n_{O^+} > 100$ cm^{-3} and red $n_{O^+} > 120$ cm^{-3}. The Jovian plasma velocity is color-coded in XY and XZ 2D cuts. The flow direction is shown by arrows along Galileo's trajectory.

fully account for particle dynamics. However, Rubin et al. (2015) observes an upstream/downstream asymmetry due to the representation of the atmosphere, which is not spherically symmetrical and accounts for a weaker downstream atmosphere. This asymmetry is not observed in RUN A1.

Arnold et al. (2019); Arnold, Liuzzo, and Simon (2020), Arnold, Simon, and Liuzzo (2020) and Addison et al. (2021) used another hybrid model to study the Europa-Magnetosphere interaction. Arnold, Liuzzo, and Simon (2020), Arnold, Simon, and Liuzzo (2020) used a magnetic field oriented only in B_z, a magnetospheric density of 60 cm^{-3}, and injected a water vapor plume from the upstream side of Europa. Addison et al. (2021) used a magnetic field $B = (0, -210, -410)$ nT, a magnetospheric density of 40 cm^{-3}, and did not inject a plume into the atmosphere. The density of O_2^+ ions is about 10^3 cm^{-3} near the surface and in the wake. Similar

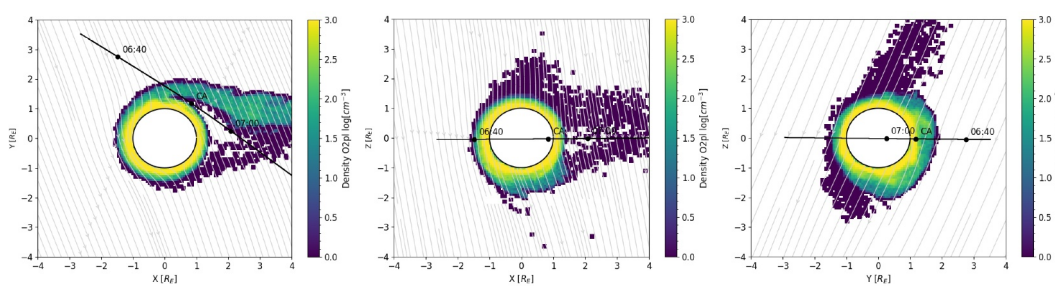

(a) $n_{O_2^+}$ in XY plane (b) $n_{O_2^+}$ in XZ plane (c) $n_{O_2^+}$ in YZ plane

Figure 4. Ionospheric density for RUN A1. From left to right, the equatorial plane (XY), the XZ plane and the YZ plane are represented. The magnetic field lines are shown in light gray.

21699402, 2025, 11, Downloaded from https://agupubs.onlinelibrary.wiley.com/doi/10.1029/2025JA033740 by Uppsala Universitet, Wiley Online Library on [04/12/2025]. See the Terms and Conditions (https://onlinelibrary.wiley.com/terms-and-conditions) on Wiley Online Library for rules of use; OA articles are governed by the applicable Creative Commons License

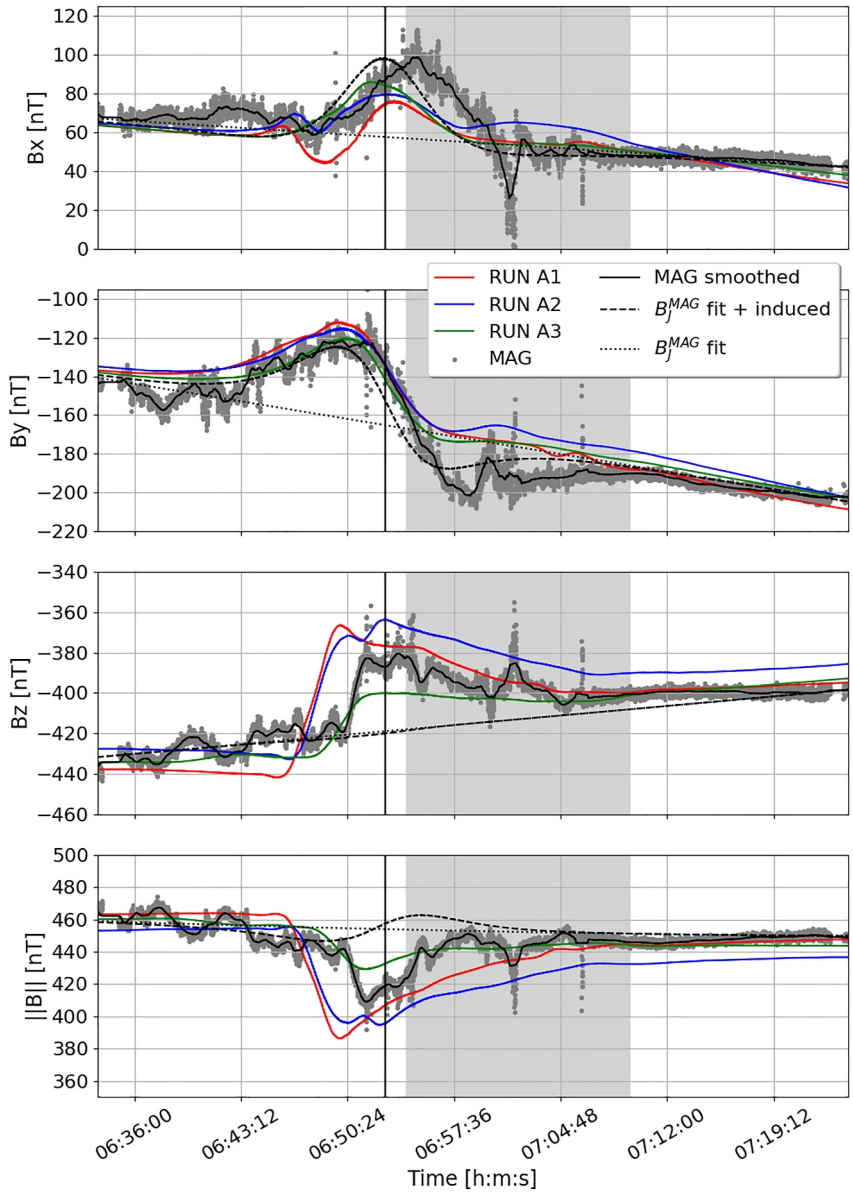

Figure 5. Magnetic field's comparison of RUNs A1, A2 and A3 with Galileo magnetometer's data. The MAG smoothed data was computed with the moving average of the Galileo data on a window of 50 s. The B_J^{MAG} fit is the linear fit of the MAG data without the interaction with Europa.

results are found with RUN A1. This order of magnitude is also found in the ionosphere but the wake is less dense. This difference may be due to the higher magnetospheric density, and also to the neutral density used by Arnold, Liuzzo, and Simon (2020), Arnold, Simon, and Liuzzo (2020) being denser, it led to a higher production of ionospheric ions. This effect is shown by Harris et al. (2021, 2022). It may also come from the electric field in the ionosphere, which is slightly weak above 100–200 km in altitude compared to results shown by Addison et al. (2021) and prevent ions from escaping (Figure 7g).

Figure 4 also emphasizes a clear asymmetry of the ionospheric tail with respect to the direction of the convective electric field $\mathbf{E} = -\mathbf{v} \times \mathbf{B}$. With the Jovian magnetic field orientation used, the convective electric field has a dominant component along the $-Y$ direction, and the equatorial plane mainly exhibits such asymmetric structure. The hemisphere in which the motional electric field points toward Europa is referred to as $E-$ hemisphere (roughly Jupiter's facing hemisphere, $Y > 0$), whereas the hemisphere where the electric field is pointing away

21699402, 2025, 11, Downloaded from https://agupubs.onlinelibrary.wiley.com/doi/10.1029/2025JA033740 by Uppsala Universitet, Wiley Online Library on [04/12/2025]. See the Terms and Conditions (https://onlinelibrary.wiley.com/terms-and-conditions) on Wiley Online Library for rules of use; OA articles are governed by the applicable Creative Commons License

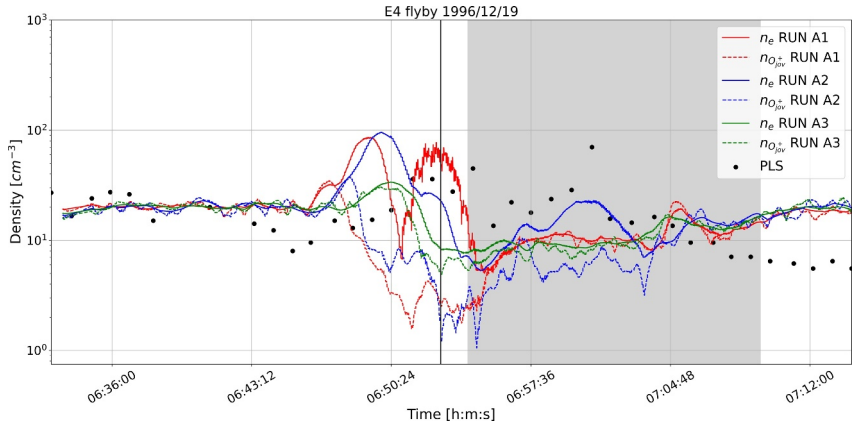

Figure 6. Density's comparison of RUNs A1, A2 and A3 with Galileo PLS's data.

from Europa is called the $E+$ hemisphere (roughly the anti-Jovian side, $Y<0$). Simulation results exhibit an ionospheric tail shifted in the $E-$ hemisphere with a sharp boundary layer at the interface with the Jovian plasma. Similar asymmetry has been characterized for other moon-magnetosphere interaction, like in Titan's environment (Simon et al., 2006). In the $E-$ hemisphere, the convective electric field in the Jovian plasma is directed perpendicular to the ionospheric tail boundary, pointing inside the tail. Ionospheric ions in the tail are thus forbidden to cross the boundary layer from inward to outward the tail. In addition, an electron gradient pressure arising from this density variation points inward the tail ($-Y$ direction), leading to an electric field term ($-\nabla \mathbf{P_e}$) in the $+Y$ direction, preventing Jovian ions from crossing from outward the tail to inward the tail.

Figures 5 and 6 show a comparison between the spacecraft data and simulation data (RUNs A1, A2 and A3) along the trajectory. During the flyby, the magnetic field evolves due to Jupiter's rapid rotation. However, the simulations are performed with a fixed value of the Jovian field. We assume that the characteristic timescales of the Europa-Jupiter interaction are shorter than the timescales for the Jovian field evolution. Indeed, $600\Omega_{O^+}^{-1} \approx 600 * 0.37 \approx 222$ s, which is well below the 50-min flyby time. To account for this evolution, we add the Jovian field's temporal dependence when plotting the curves. We proceeded as follow: we assumed a linear evolution of the Jovian magnetic field and we computed the linear fit of B_j^{MAG} with two points, one before and one after the interaction with Europa in order to remove the part resulting of the interaction with the moon in Galileo's magnetometer data. Then we added to the simulation data the difference between the fixed value of B_j^{sim} used in the simulation (see Table 4) and the linear fit of B_j^{MAG}. This linear fit is shown as the dotted black curves in Figure 5.

The B_x and B_y components of the magnetic field (Figure 5) are dominated by Europa's induced magnetic field. Indeed, both components vary close to the CA, following the variations of the dashed black line representing the Jovian and induced magnetic field, before returning to their ambient magnetic field value when the probe crosses and exits the wake. The induced field has a minor contribution to the B_z component because the dipole representing it is oriented only in the XY plane in which the trajectory takes part. Additionally, the E4 flyby occurred in the quasi-equatorial plane with a very slight inclination on the Z axis. Thus, the B_z perturbation is due to the magnetic field associated with plasma interaction. The magnetometer measured a sudden decrease in magnitude, just before the CA, before slowly returning to the ambient magnetic field values. The simulation shows the same phenomenon but shifted by a few minutes in the case of the RUN A1. This signature is associated to the draping of the magnetic field lines and its location might vary according to the effective size of the obstacle. A denser ionosphere will present a larger effective obstacle. The increase in the B_z component upstream of Europa illustrates the stacking of magnetic field lines upstream of the ionospheric layers. This is due to the interaction with the plasma and the asymmetric ionospheric escape on the pro-Jovian side.

Figure 6 shows the electron density of RUN A1 (in red) and the density observed by Galileo (in black). In RUN A1, two peaks in electron density are visible around 6h50. The first peak corresponds to the escape tail, and the second peak corresponds to a passage through the ionosphere. Harris et al. (2021), who performed MHD simulations with the same parameters except for the ionosphere initialization, have a density peak in the wake,

21699402, 2025, 11, Downloaded from https://agupubs.onlinelibrary.wiley.com/doi/10.1029/2025JA033740 by Uppsala Universitet, Wiley Online Library on [04/12/2025]. See the Terms and Conditions (https://onlinelibrary.wiley.com/terms-and-conditions) on Wiley Online Library for rules of use; OA articles are governed by the applicable Creative Commons License

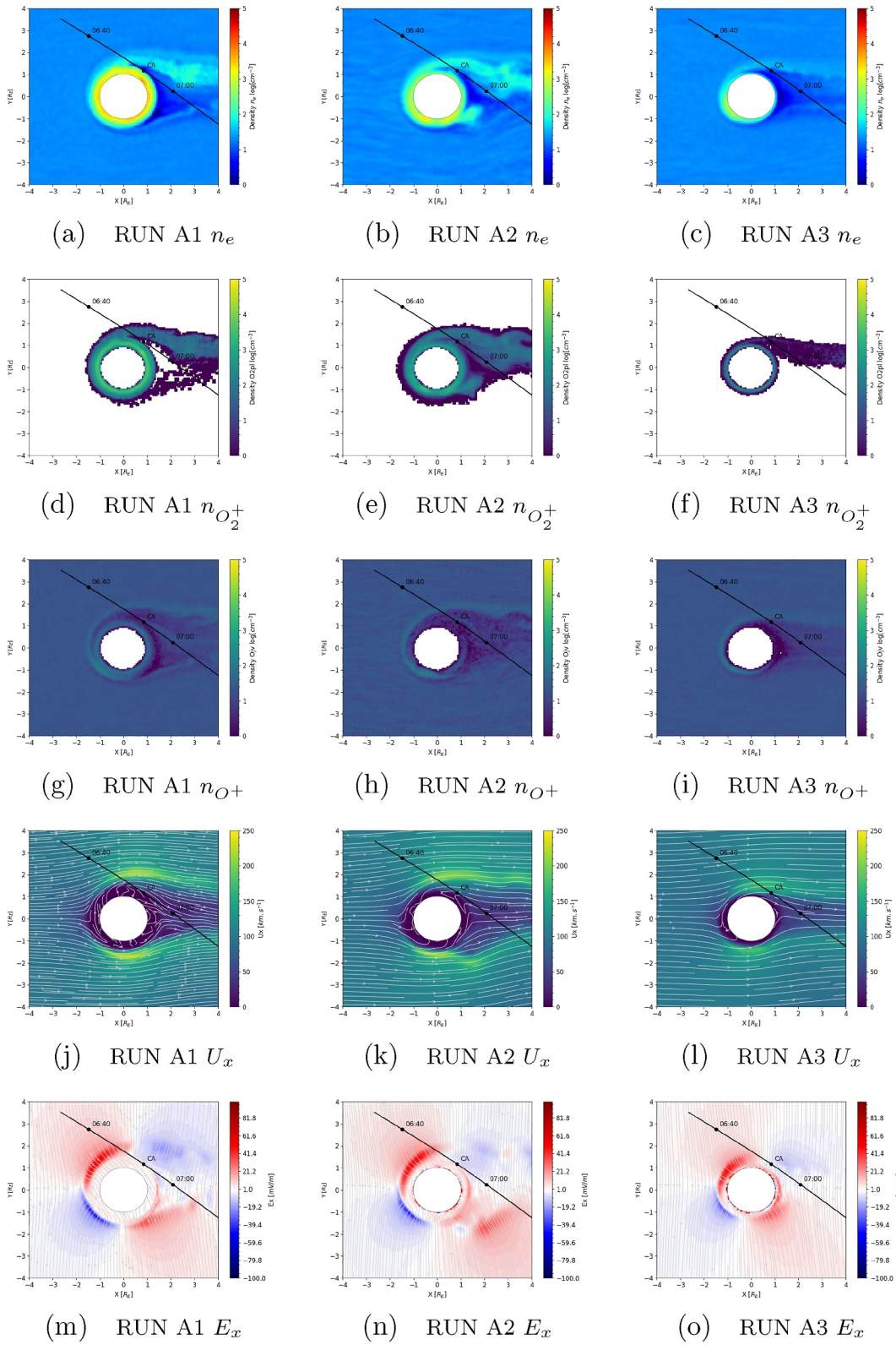

Figure 7. Electron, planetary $n_{O_2^+}$ and jovian n_{O^+} densities, velocity and E_x in the equatorial plane for the simulations A1, A2 and A3.

21699402, 2025, 11, Downloaded from https://agupubs.onlinelibrary.wiley.com/doi/10.1029/2025JA033740 by Uppsala Universitet, Wiley Online Library on [04/12/2025]. See the Terms and Conditions (https://onlinelibrary.wiley.com/terms-and-conditions) on Wiley Online Library for rules of use; OA articles are governed by the applicable Creative Commons License

21699402, 2025, 11, Downloaded from https://agupubs.onlinelibrary.wiley.com/doi/10.1029/2025JA033740 by Uppsala Universitet, Wiley Online Library on [04/12/2025]. See the Terms and Conditions (https://onlinelibrary.wiley.com/terms-and-conditions) on Wiley Online Library for rules of use; OA articles are governed by the applicable Creative Commons License

correlated with a density peak measured by Galileo (around 7:00). The peak they obtain is about 80 cm^{-3}, and in the RUN A1, the escape tail peak is also about 80 cm^{-3}. A second peak around CA has been measured by Galileo, about 40 cm^{-3}, which could correspond to the spacecraft passing through the ionosphere and is thus represented by the LatHyS simulation. The MHD simulation of Harris et al. (2021) does not reproduce this density peak. A decrease in Jovian ion density is observed when the probe crosses the wake.

Several conclusions can be drawn from this comparison. First, there may be some concerns regarding the particle instruments PLS, as they could face challenges in accurately sampling low-energy ions (with energy resolution less than a few eV) and might be affected by satellite potential effects, potentially impacting the measurement of the ionospheric ion densities and velocities. For example, Paterson et al. (1999) noted that the density peak in the geometric wake (around 7:00) is probably O_2^+ ions. However, in the analysis to derive the density and velocity from the measurements, they chose to combine the distributions of different major Jovian ions (H^+, O^+, O^{2+}, S^{2+}, S_2^+). Thus, Paterson et al. (1999) reports that by choosing a pure distribution of O_2^+ in the wake, the density would be about 60% larger, and the velocity would be about 40% smaller. This would bring the velocity observations closer to the simulation results. Furthermore, limited information on the plasma composition has been derived during this flyby. The incoming plasma composition might play a role in the interaction (through charge exchange reactions). Finally, the assumption about the ionosphere used in RUN A1 based on radio occultation observations can be improved (ionosphere too dense or too extended).

Overall, RUN A1 successfully replicates the main features observed by Galileo, though some discrepancies suggest that certain parameters are not fully captured. This is particularly evident in the representation of the ionosphere and the neutral environment. Asymmetries in the atmosphere and ionosphere are not addressed in this simulation, and only O_2^+ ions are considered. Consequently, it is worthwhile to explore the system's sensitivity to changes in the neutral and ionospheric environments.

4.1.2. Comparison Analytical Description Versus EGM

Two additional simulations were conducted with the same plasma and magnetic field parameters of RUN A1 (see Table 4). The neutral and ionospheric environment at initialization varied from a purely analytical description to a modeled description. These simulations are referred to as A1, A2, and A3, as summarized in Table 5. The case "Analytical" represents the analytical description of the atmosphere (Section 2.2.1) and ionosphere (Section 2.4.1). The atmosphere can also be described using the EGM exosphere model (Section 2.2.2). Finally, a method is employed to construct the ionosphere by calculating ion production over an integration time of 10 $\Omega_{O^+}^{-1}$, rather than relying on an analytical model (Section 2.4.2). This approach results in a self-consistent atmosphere/ionosphere (run A2 using an analytical model for the neutral atmosphere and RUN3 using EGM neutral atmosphere).

The general dynamics of the three simulations remain the same as discussed earlier. Figures 7a–7c show the density for the three simulations in the equatorial plane. The next two rows in the figure separately highlight the planetary O_2^+ ions (Figures 7d, 7e, and 7f) and Jovian O^+ (Figures 7g–7i). Similar pro-Jovian escape patterns are observed, as noted in RUN A1. The main difference lies in the decreasing density as we move toward a modeled atmosphere/ionosphere. In RUN A1, the ionosphere is constructed using an analytical model with spherical symmetry, where the height scales are 240 km, from the surface to 300 km in altitude, and then 440 km, up to 600 km in altitude. Thus, there is a very extended ionosphere with a density of approximately 100 cm^{-3} even beyond 300 km in altitude. The surface density at initialization is 2500 cm^{-3} for all three simulations. The ionosphere in RUN A2 is built from the atmosphere, which is derived from a spherically symmetric profile with a height scale of 100 km. Thus, the ionosphere mirrors the atmosphere with an equivalent height scale. Consequently, the ionosphere is slightly less extended. In the last RUN A3, the ionosphere is constructed similarly to RUN A2 but from an atmosphere derived from EGM. The O_2 atmosphere (Figure 2) is not very extended, with a height scale of less than 20 km, reaching a few kilometers near the surface. This directly impacts the ionosphere, especially considering the spatial resolution of the simulations is 100 km, resulting in less accurate density representation (Figures 7d, 7e, and 7f). Two additional species were included in RUN A3: H_2O^+ and H_2^+, but they have a negligible impact on currents and fields due to their much lower density. Water atmosphere (Figure 2) exhibits strong asymmetries as it originates from surface sublimation and sputtering. During the E4 flyby, the local time was 17 hr, so the Sun was nearly pointing in the -X direction, and photons had an almost colinear direction with the Jovian plasma flow. Thus, there is an increase in H_2O density upstream of Europa. Hydrogen

Table 6
Parameters of the Different Simulations

	RUN B1	RUN B2	RUN C1	RUN C2
Plasma parameters	JUICE 7E1	JUICE 7E1	JUICE 8E2	JUICE 8E2
Exosphere model	Analytical	EGM	Analytical	EGM
Ionosphere model	Self-consistent	Self-consistent	Self-consistent	Self-consistent

Note. Refer to Table 4 for the plasma parameters of each flybys. The Analytical descriptions for atmosphere/ionosphere are described in Sections 2.2.1 and 2.4.1. The EGM model used for the neutral environment is described in Section 2.2.2 and the self-consistent ionosphere is detailed in Section 2.4.2.

(H_2) (Figure 2) and H_2^+ are relatively light and volatile, with density lower than that of O_2 and O_2^+. However, the height scale is large, exceeding 400 km, making the hydrogen atmosphere and production of this ionic species extensive.

Szalay et al. (2024) reported direct observations of H_2^+ pickup ions by Juno's Jovian Auroral Distributions Experiment (JADE) during the Europa flyby of 29 September 2022. Juno transited the geometric wake with a closest approach of 353 km. They determined a H_2^+ density in the wake of around 10 cm^{-3}, peaking at $\sim$60 cm^{-3} at closest approach. Although the geometry of the Juno flyby is similar to the Galileo E4 flyby, the magnetospheric plasma density is 5 times greater, reaching 100 cm^{-3} compared to the 20 cm^{-3} measured during the Galileo flyby. The production of H_2^+ by electronic impact is therefore greater under these conditions. RUN A3 shows an extensive escape of H_2^+ in the wake with a fairly low density of about 1 cm^{-3} which can rise to over 10 cm^{-3} with the escape of ions from the upstream ionosphere. The H_2^+ density in the wake for the JUICE simulations where the magnetospheric plasma density is 100 cm^{-3}, discussed in Section 4.2, are close to those determined by Szalay et al. (2024). The observations of H_2^+ by Juno's flyby and the simulations tends to show that H_2^+ seen in the Jovian plasma could originate from Europa, especially since the density monotonously decreases with radial distance (Szalay et al., 2024) and does not show an increase near Ganymede's orbit (Szalay et al., 2022).

The initialized ionosphere plays a crucial role as it determines the intensity of currents. The neutrals have a negligible velocity ($\approx$100 m s^{-1}) compared to the Jovian ions ($\approx$100 km s^{-1}) and we inject ionospheric macroparticles at rest. Figures 7m–7o show the differences in the electric field, particularly the boundary of the ionosphere where the electric field is very weak (<1 mV/m). The same observation can be made in Figures 7j, 7k, and 7l, which show the flow around the obstacle.

Figure 5 shows that the simulations give very similar trends. RUN A3 shows B_x and B_y closer to Galileo's observations, but B_z has a weaker jump due to the low density of the ionosphere.

Finally, in the density comparison Figure 6, which compares electron density and Jovian ion density, each simulation shows a density peak around 6:50 a.m., corresponding to the passage through the ionospheric tail. RUN A2 also shows a density peak in the wake at around 7:00, similar to the density peak observed by Galileo.

In conclusion, the ideal simulation would lie between the results of RUNs A2 and A3. However, there is a bias related to the spatial resolution of 100 km. This resolution does not perfectly describe the ionospheric dynamics because only 6 cells (600 km) are used to describe this region. In the case of RUN A3, the scale height is significantly lower, making the representation less accurate. Moreover, a large spatial scale does not allow for accurate tracking of ion flow, especially the ionospheric flow from upstream to downstream.

4.2. JUICE Flybys

Simulations were performed to analyze and predict the future observations of JUICE during the 7E1 and 8E2 Europa flybys based on CReMA 5.1 (Consolidated Report on Mission Analysis) trajectories. Simulations parameters are reported in Tables 4 and 6 where RUN B1 and B2 correspond to 7E1 flyby and RUN C1 and C2 to 8E2 flyby.

Simulations were performed with the same simulation characteristics than RUN A1 except that the spatial resolution is $\Delta x = 0.5c/\omega_{pi} = 90$ km. We used $250 \times 600 \times 600$ grid points and about 9×10^8 particles.

21699402, 2025, 11, Downloaded from https://agupubs.onlinelibrary.wiley.com/doi/10.1029/2025JA033740 by Uppsala Universitet, Wiley Online Library on [04/12/2025]. See the Terms and Conditions (https://onlinelibrary.wiley.com/terms-and-conditions) on Wiley Online Library for rules of use; OA articles are governed by the applicable Creative Commons License

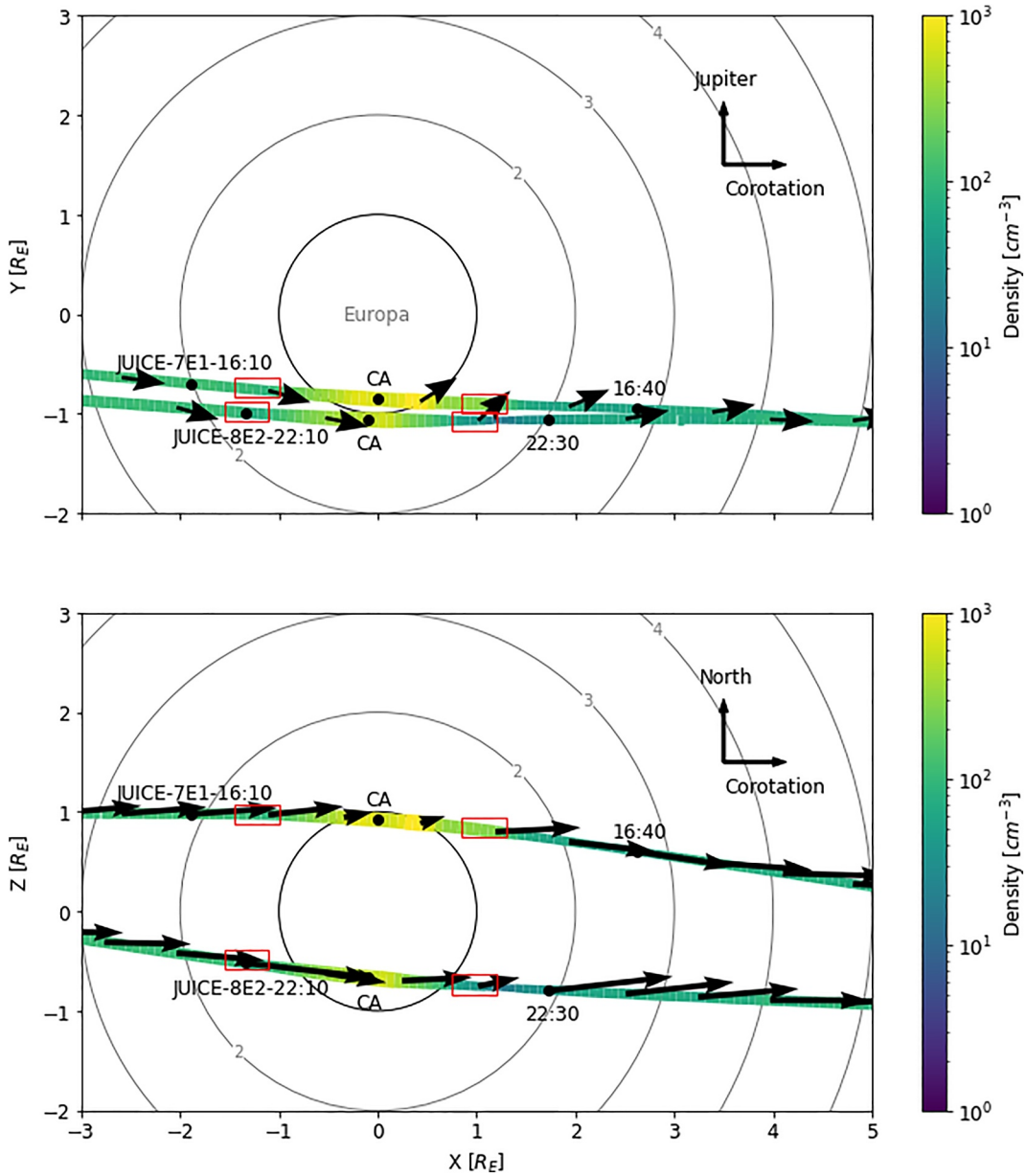

Figure 8. This figure shows the variation in density measured along JUICE's 7E1, 8E2 flybys, simulated with configurations B2 and C2. The arrows represent the overall particle velocity along the flybys, scaled by the Jovian plasma velocity of 100 km s^{-1}. The red rectangles indicate the boundary separating the Jovian upstream plasma region from the ionospheric region as shown in Figures 9 and 10 (gray areas).

Run B1/C1 and B2/C2 (Table 6) follow the same approach for the neutral description than RUN A2/A3 (analytical profile/3D EGM atmosphere).

In all of these simulations the ionosphere is self-consistently generated.

We focus on the future observations of JUICE during the two flybys (see Table 4 for JUICE flybys information). In each graphs, the red curves correspond to the 7E1 flyby, and the black curves correspond to the 8E2 flyby. To simplify the interpretation of the curves, the time axis is defined with respect to the closest approach, indicated by the black vertical line.

During the flybys, JUICE will explore different region of Jupiter-Europa interaction, from the Jovian upstream plasma region to Europa's wake, including a region governed by planetary plasma. From Figures 9 and 10, a sharp

21699402, 2025, 11, Downloaded from https://agupubs.onlinelibrary.wiley.com/doi/10.1029/2025JA033740 by Uppsala Universitet, Wiley Online Library on [04/12/2025]. See the Terms and Conditions (https://onlinelibrary.wiley.com/terms-and-conditions) on Wiley Online Library for rules of use; OA articles are governed by the applicable Creative Commons License

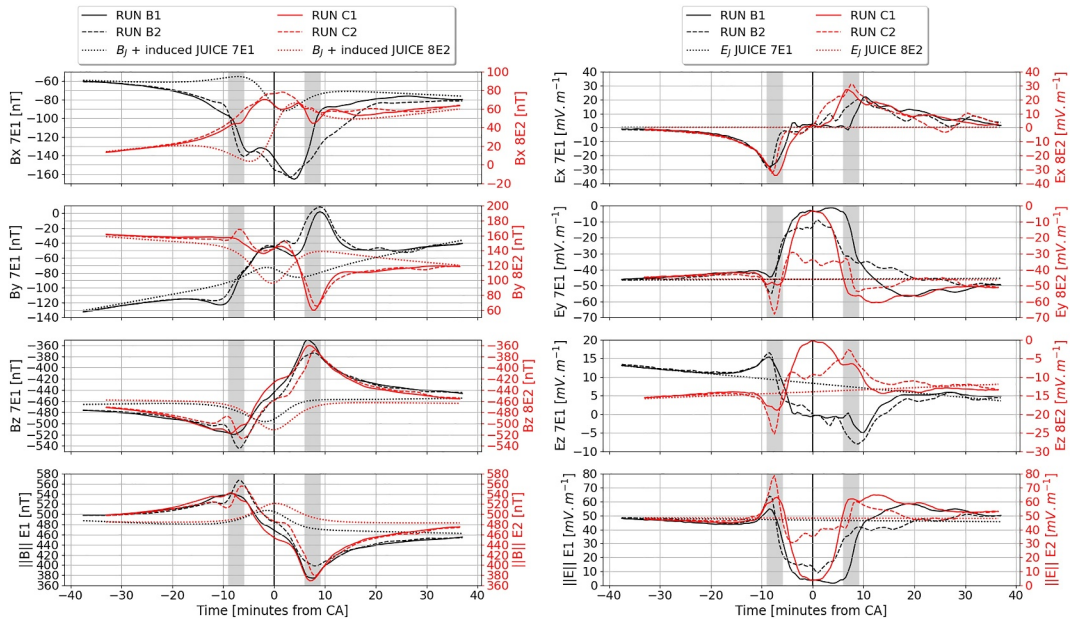

Figure 9. Magnetic and Electric field simulated along JUICE flybys 7E1 and 8E2. The gray areas indicate the boundary separating the Jovian upstream plasma region from the ionospheric region as shown in Figure 8 (red rectangles).

change in electron number density, associated to a sharp decrease of the electric field is clearly seen and correspond to a time when the plasma composition is modified. In Figure 8, showing the velocity along the flybys, the ionospheric region is crossed by the spacecraft where the velocity decreases and the density increases. These transition regions are highlighted by red rectangles in Figure 8 and gray areas in Figures 9 and 10.

Figure 9 depicts the magnetic field and electric field along JUICE flybys. The simulation data plotted in this figure take into account the evolution of the Jovian magnetic field. The Jovian field's temporal dependence is added using the same methodology as described in Section 4.1.1 when discussing Figure 5. On the left graph, the dashed curves show the ambient and induced Jovian magnetic fields. It can be observed that the magnetic field is hardly dominated by the induced field, but by the interaction with the ionosphere. The signatures of entry and exit from the ionosphere at CA-10 and CA + 10 min can be observed. On the right graph, the electric field is plotted, giving information on the amplitude that could be measured during the flybys.

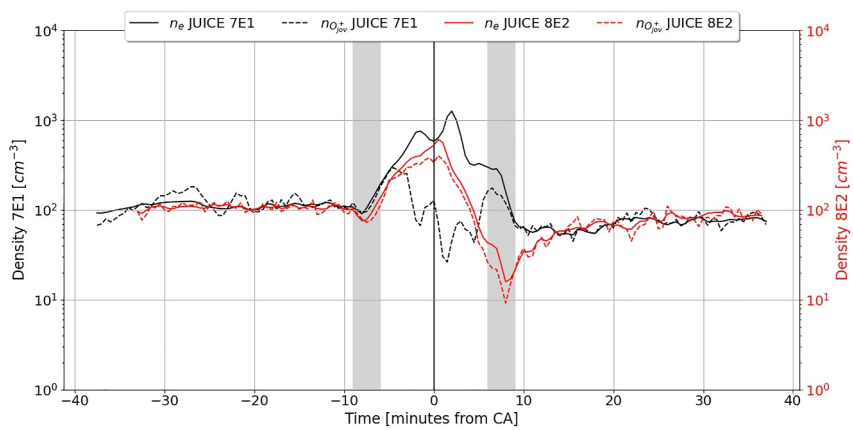

Figure 10. Electron density simulated along JUICE 7E1 and 8E2 flybys. Black curves refer to RUN B2 and red curves to RUN C2. The gray areas indicate the boundary separating the Jovian upstream plasma region from the ionospheric region as shown in Figure 8 (red rectangles).

21699402, 2025, 11, Downloaded from https://agupubs.onlinelibrary.wiley.com/doi/10.1029/2025JA033740 by Uppsala Universitet, Wiley Online Library on [04/12/2025]. See the Terms and Conditions (https://onlinelibrary.wiley.com/terms-and-conditions) on Wiley Online Library for rules of use; OA articles are governed by the applicable Creative Commons License

21699402, 2025, 11, Downloaded from https://agupubs.onlinelibrary.wiley.com/doi/10.1029/2025JA033740 by Uppsala Universitet, Wiley Online Library on [04/12/2025]. See the Terms and Conditions (https://onlinelibrary.wiley.com/terms-and-conditions) on Wiley Online Library for rules of use; OA articles are governed by the applicable Creative Commons License

Figure 10 shows the measured density during the flybys. The density peak of 10^3 cm^{-3} is observed at CA (401 km). On the 8E2 flyby curves (in black), the density decreases and becomes lower than the incident plasma density, corresponding to a region in the wake crossed by JUICE. It is notable that the simulation predicts a high density of Jovian ions in this region (dotted black curve), reaching at least 500 cm^{-3}, approaching the density of ionospheric O_2^+ ions.

5. Discussion

The Jupiter-Europa simulation model has been validated through simulations under the conditions of the E4 flyby, replicating the main features observed by Galileo (magnetic field, velocity, and density). Comparisons with velocity and density indicate a pro-jovian shift of the tail, a result not found in MHD simulation outcomes (Harris et al., 2021).

Three neutral/ionospheric environment models were compared, in order to observe the system's response to their variations. It was noted that the ionosphere influences the magnetic field intensity. Using an atmosphere derived from a planetary exosphere simulation model like EGM allows to consider various asymmetries and multiple major neutral species which will be useful for further studies on ionospheric ions dynamics.

Following this, simulations were conducted for the JUICE flybys 7E1 and 8E2, scheduled for 2032. Magnetospheric conditions are determined by models, and the JUICE simulations show ionospheric densities close to those observed by radio occultations during the Galileo mission (around 10^4 cm^{-3}) whereas the ionospheric densities resulting in RUNs A2 and A3 are below the estimations obtained from radio occultations. This suggests that the magnetospheric environment is a crucial parameter to consider, the dynamic of the ionosphere, mostly generated by electronic impact, is related to the incident plasma conditions (density, temperature, velocity) and to the exospheric density and composition. This is also supported by Harris et al. (2021), who studied the system's response, particularly the precipitation of magnetospheric ions, to variations in external plasma conditions. They demonstrated that jovian ion surface precipitation is sensitive to changes, especially in the incident plasma density. This is further supported by density maps indicating significant ion production upstream and consequently more substantial precipitation.

Subsequently, measurements of the magnetic field, velocity, and density were plotted along the JUICE flybys. It is worth noting that the spacecraft crosses the ionospheric region governed by planetary plasma where a sharp change in electron number density associated to a modification in the plasma composition, and a sharp decrease of the electric field is observed. The measured signatures primarily depend on interactions with this region.

Simulations with LatHyS with smaller spatial resolution, allowing for better consideration of ionospheric scale heights, seem to be the preferred direction for future studies to better characterize this region of interest, near Europa and particularly its ionosphere. Europa's ionosphere is limited (approximately 600 km altitude) and is where most interactions occur. The ideal resolution would be to tend toward the resolution of EGM's near surface cells (<10 km) and toward that proposed by MHD models (~10–20 km near the surface), which is a great computational challenge with hybrid models like LatHyS, so aiming for a resolution of 50 km in the $4R_E$ region around Europa would already greatly improve the description of ionospheric dynamics. With this in view, it becomes interesting and relevant to study the dynamics of the various ionospheric species from simulations using EGM.

Furthermore, it is essential to investigate the impact of active processes on Europa's surface, such as potential plumes. EGM allows to model a water plume ejection and it would be interesting to explore what measurements the JUICE spacecraft would make if such a phenomenon were to occur before or during a flyby. Some works had already been done using MHD simulations (Blöcker et al., 2016; Jia et al., 2018) and hybrid simulations (Addison et al., 2021; Arnold et al., 2019, 2020). However, none of them uses a Monte-Carlo exosphere model that can take into account this phenomenon or apply it to future JUICE observations.

Conflict of Interest

The authors declare no conflicts of interest relevant to this study.

21699402, 2025, 11, Downloaded from https://agupubs.onlinelibrary.wiley.com/doi/10.1029/2025JA033740 by Uppsala Universitet, Wiley Online Library on [04/12/2025]. See the Terms and Conditions (https://onlinelibrary.wiley.com/terms-and-conditions) on Wiley Online Library for rules of use; OA articles are governed by the applicable Creative Commons License

Data Availability Statement

The Galileo Magnetometer data for the Europa flybys were obtained from the NASA Planetary Data System and the JUICE trajectories are based on the kernels CReMA 5.1 proposed by the ESA Space Operation Center (SOC). Results from the LatHyS hybrid model presented in this publication can be downloaded online (http://impex.latmos.ipsl.fr/). The simulation used for RUN A1 is Europa_22_03_23, the one used for RUN A2 is Europa_22_06_23 and for RUN A3 is Europa_19_04_23. For RUN B1 and B2, the simulations used are Europa_J7E1_09_08_23 and Europa_J7E1_09_05_23 respectively. And for RUN C1 and C2, the simulations used are Europa_J8E2_08_08_23 and Europa_J8E2_09_05_23 respectively.

Acknowledgments

B. Baskevitch, R. Modolo and B. Cecconi are grateful to DIM ACAV + for financial support of this project. F. Leblanc was supported by the project FACOM (ANR-22-CE49-0005-01 ACT). This work was supported by CNES, through the Soleil-Heliosphere-Magnetosphere program. The authors thank the JUICE RPWI team for useful discussions on this work. High-performance computing resources supporting this work were provided by MesoPSL (https://wwwmesopsl-new.obspm.fr/) and ESPRI (https://documentations.ipsl.fr/spirit/index.html) computing and data centers.

References

Addison, P., Liuzzo, L., Arnold, H., & Simon, S. (2021). Influence of Europa's time-varying electromagnetic environment on magnetospheric ion precipitation and surface weathering. *Journal of Geophysical Research: Space Physics*, *126*(5), e2020JA029087. https://doi.org/10.1029/2020JA029087

Aizawa, S., Persson, M., Menez, T., André, N., Modolo, R., Génot, V., et al. (2022). Lathys global hybrid simulation of the bepicolombo second Venus flyby. *Planetary and Space Science*, *218*, 105499. https://doi.org/10.1016/j.pss.2022.105499

Allegrini, F., Saur, J., Szalay, J. R., Ebert, R. W., Kurth, W. S., Cervantes, S., et al. (2024). Electron beams at Europa. *Geophysical Research Letters*, *51*(13), e2024GL108422. https://doi.org/10.1029/2024GL108422

Arnold, H., Liuzzo, L., & Simon, S. (2019). Magnetic signatures of a plume at Europa during the Galileo E26 flyby. *Geophysical Research Letters*, *46*(3), 1149–1157. https://doi.org/10.1029/2018GL081544

Arnold, H., Liuzzo, L., & Simon, S. (2020). Plasma interaction signatures of plumes at Europa. *Journal of Geophysical Research: Space Physics*, *125*(1), e2019JA027346. https://doi.org/10.1029/2019JA027346

Arnold, H., Simon, S., & Liuzzo, L. (2020b). Applying ion energy spectrograms to search for plumes at Europa. *Journal of Geophysical Research: Space Physics*, *125*(9), e2020JA028376. https://doi.org/10.1029/2020JA028376

Bagenal, F., & Dols, V. (2020). The space environment of IO and Europa. *Journal of Geophysical Research: Space Physics*, *125*(5), e2019JA027485. https://doi.org/10.1029/2019JA027485

Bagenal, F., Sidrow, E., Wilson, R. J., Cassidy, T. A., Dols, V., Crary, F. J., et al. (2015). Plasma conditions at Europa's orbit. *Icarus*, *261*, 1–13. https://doi.org/10.1016/j.icarus.2015.07.036

Banks, P. M., & Kockarts, G. (1973). Aeronomy.

Barabash, S. e. a. (2025). The particle environment package (pep) for the Jupiter icy moons explorer (juice). *Space Science Reviews*. [Manuscript in preparation].

Beth, A., Galand, M., Modolo, R., Jia, X., Leblanc, F., & Huybrighs, H. L. F. (2025). Ionosphere of Ganymede: Galileo observations versus test particle simulation. *Monthly Notices of the Royal Astronomical Society*, *538*(4), 2483–2507. https://doi.org/10.1093/mnras/staf313

Blöcker, A., Saur, J., & Roth, L. (2016). Europa's plasma interaction with an inhomogeneous atmosphere: Development of Alfvén winglets within the Alfvén wings. *Journal of Geophysical Research: Space Physics*, *121*(10), 9794–9828. https://doi.org/10.1002/2016JA022479

Carnielli, G., Galand, M., Leblanc, F., Leclercq, L., Modolo, R., Beth, A., et al. (2019). First 3d test particle model of ganymede's ionosphere. *Icarus*, *330*, 42–59. https://doi.org/10.1016/j.icarus.2019.04.016

Cassidy, T., Paranicas, C., Shirley, J., Dalton III, J., Teolis, B., Johnson, R., et al. (2013). Magnetospheric ion sputtering and water ice grain size at Europa. *Planetary and Space Science*, *77*, 64–73. https://doi.org/10.1016/j.pss.2012.07.008

Connerney, J. E. P., Kotsiaros, S., Oliversen, R. J., Espley, J. R., Joergensen, J. L., Joergensen, P. S., et al. (2018). A new model of Jupiter's magnetic field from Juno's first nine orbits. *Geophysical Research Letters*, *45*(6), 2590–2596. https://doi.org/10.1002/2018GL077312

Cravens, T. E., Kozyra, J. U., Nagy, A. F., Gombosi, T. I., & Kurtz, M. (1987). Electron impact ionization in the vicinity of comets. *Journal of Geophysical Research*, *92*(A7), 7341–7353. https://doi.org/10.1029/JA092iA07p07341

Dougherty, M. K. e. a. (2025). The j-mag magnetometer for the Jupiter icy moons explorer (juice). *Space Science Reviews*. [Manuscript in preparation].

Hansen, C. J., Shemansky, D. E., & Hendrix, A. (2005). Cassini uvis observations of Europa's oxygen atmosphere and torus. *Icarus*, *176*(2), 305–315. https://doi.org/10.1016/j.icarus.2005.02.007

Harris, C. D. K., Jia, X., & Slavin, J. A. (2022). Multi-fluid mhd simulations of Europa's plasma interaction: Effects of variation in Europa's atmosphere. *Journal of Geophysical Research: Space Physics*, *127*(9), e2022JA030569. https://doi.org/10.1029/2022JA030569

Harris, C. D. K., Jia, X., Slavin, J. A., Toth, G., Huang, Z., & Rubin, M. (2021). Multi-fluid MHD simulations of Europa's plasma interaction under different magnetospheric conditions. *Journal of Geophysical Research: Space Physics*, *126*(5), e2020JA028888. https://doi.org/10.1029/2020JA028888

Hoffman, J. M., Miller, G. H., & Lockwood, G. J. (1982). Charge transfer of ground-state C+, N+, and O+ in N2 and H2. *Physics Reviews*, *25*(4), 1930–1936. https://doi.org/10.1103/PhysRevA.25.1930

Howell, S. M. (2021). The likely thickness of Europa's icy shell. *The Planetary Science Journal*, *2*(4), 129. https://doi.org/10.3847/PSJ/abfe10

Hwang, W., Kim, Y., & Rudd, M. E. (1996). New model for electron-impact ionization cross sections of molecules. *The Journal of Chemical Physics*, *104*(8), 2956–2966. https://doi.org/10.1063/1.471116

Jia, X., Kivelson, M., Khurana, K., & Kurth, W. (2018). Evidence of a plume on Europa from Galileo magnetic and plasma wave signatures. *Nature Astronomy*, *2*(6), 459–464. https://doi.org/10.1038/s41550-018-0450-z

Johnson, R., Burger, M., Cassidy, T., Leblanc, F., Marconi, M., & Smyth, W. (2009). Composition and detection of Europa's sputter-induced atmosphere.

Kabin, K., Combi, M. R., Gombosi, T. I., Nagy, A. F., DeZeeuw, D. L., & Powell, K. G. (1999). On europa's magnetospheric interaction: A mhd simulation of the e4 flyby. *Journal of Geophysical Research*, *104*(A9), 19983–19992. https://doi.org/10.1029/1999JA900263

Kallio, E., Chaufray, J.-Y., Modolo, R., Snowden, D., & Winglee, R. (2011). Modeling of Venus, Mars, and Titan. *Space Science Reviews*, *162*(1–4), 267–307. https://doi.org/10.1007/s11214-011-9814-8

Kim, T. K., Ebert, R. W., Valek, P. W., Allegrini, F., McComas, D. J., Bagenal, F., et al. (2020). Survey of ion properties in Jupiter's plasma sheet: Juno jade-i observations. *Journal of Geophysical Research: Space Physics*, *125*(4), e2019JA027696. https://doi.org/10.1029/2019JA027696

Kivelson, M., Bagenal, F., Kurth, W., Neubauer, F., Paranicas, C., & Saur, J. (2004). Magnetospheric interactions with satellites. *The Planet, Satellites and Magnetosphere*, 513–536.
Kivelson, M., Khurana, K., Russell, C., Volwerk, M., Walker, R., & Zimmer, C. (2000). 09). Galileo magnetometer measurements: A stronger case for a subsurface ocean at europa. *Science*, *289*, 1340-3. https://doi.org/10.1126/science.289.5483.1340
Kivelson, M., Khurana, K., & Volwerk, M. (2009). Europa's interaction with the Jovian magnetosphere.545
Kliore, A. J., Hinson, D. P., Flasar, F. M., Nagy, A. F., & Cravens, T. E. (1997). The ionosphere of Europa from Galileo radio occultations. *Science*, *277*(5324), 355–358. https://doi.org/10.1126/science.277.5324.355
Leblanc, F., Oza, A., Leclercq, L., Schmidt, C., Cassidy, T., Modolo, R., et al. (2017). On the orbital variability of ganymede's atmosphere. *Icarus*, *293*, 185–198. https://doi.org/10.1016/j.icarus.2017.04.025
Leclercq, L., Modolo, R., Leblanc, F., Hess, S., & Mancini, M. (2016). 3d magnetospheric parallel hybrid multi-grid method applied to planet–plasma interactions. *Journal of Computational Physics*, *309*, 295–313. https://doi.org/10.1016/j.jcp.2016.01.005
Ledvina, S., Ma, Y., & Kallio, E. (2008). Modeling and simulating flowing plasmas and related phenomena. *Space Science Reviews*, *139*(1–4), 143–189. https://doi.org/10.1007/s11214-008-9384-6
Lindsay, B. G., Rejoub, R., Sieglaff, D. R., & Stebbings, R. F. (2001). Charge transfer of keV O+ ions with CO and H2. *Journal of Physics B: Atomic, Molecular and Optical Physics*, *34*(11), 2159–2165. https://doi.org/10.1088/0953-4075/34/11/308
Lindsay, B. G., & Stebbings, R. F. (2005). Charge transfer cross sections for energetic neutral atom data analysis. *Journal of Geophysical Research (Space Physics)*, *110*(A12), A12213. https://doi.org/10.1029/2005JA011298
Lipatov, A., Cooper, J., Paterson, W., Sittler, E., Hartle, R., & Simpson, D. (2010). Jovian plasma torus interaction with Europa: 3d hybrid kinetic simulation. first results. *Planetary and Space Science*, *58*(13), 1681–1691. https://doi.org/10.1016/j.pss.2010.06.015
Lipatov, A., Cooper, J., Paterson, W., Sittler, E., Jr., Hartle, R., & Simpson, D. (2013). Jovian plasma torus interaction with Europa plasma wake structure and effect of inductive magnetic field: 3d hybrid kinetic simulation. *Planetary and Space Science*, *77*, 12–24. https://doi.org/10.1016/j.pss.2013.01.009
Liu, Y., Nagy, A. F., Kabin, K., Combi, M. R., DeZeeuw, D. L., Gombosi, T. I., & Powell, K. G. (2000). Two-species, 3d, mhd simulation of Europa's interaction with Jupiter's magnetosphere. *Geophysical Research Letters*, *27*(12), 1791–1794. https://doi.org/10.1029/1999GL003734
Matthews, A. P. (1994). Current advance method and cyclic leapfrog for 2d multispecies hybrid plasma simulations. *Journal of Computational Physics*, *112*(1), 102–116. https://doi.org/10.1006/jcph.1994.1084
McGrath, M., & Sparks, W. (2017). Galileo ionosphere profile coincident with repeat plume detection location at Europa. *Research Notes of the AAS*, *1*, 14. https://doi.org/10.3847/2515-5172/aa988e
Modolo, R., & Chanteur, G. M. (2008). A global hybrid model for titan's interaction with the kronian plasma: Application to the cassini ta flyby. *Journal of Geophysical Research*, *113*(A1). https://doi.org/10.1029/2007JA012453
Modolo, R., Hess, S., Mancini, M., Leblanc, F., Chaufray, J.-Y., Brain, D., et al. (2016). Mars-solar wind interaction: Lathys, an improved parallel 3-d multispecies hybrid model. *Journal of Geophysical Research: Space Physics*, *121*(7), 6378–6399. https://doi.org/10.1002/2015JA022324
Neubauer, F. M. (1980). Nonlinear standing alfvén wave current system at io: Theory. *Journal of Geophysical Research*, *85*(A3), 1171–1178. https://doi.org/10.1029/JA085iA03p01171
Neubauer, F. M. (1998). The sub-alfvénic interaction of the galilean satellites with the Jovian magnetosphere. *Journal of Geophysical Research*, *103*(E9), 19843–19866. https://doi.org/10.1029/97JE03370
Neubauer, F. M. (1999). Alfvén wings and electromagnetic induction in the interiors: Europa and callisto. *Journal of Geophysical Research*, *104*(A12), 28671–28684. https://doi.org/10.1029/1999JA900217
Oza, A. V., Johnson, R. E., & Leblanc, F. (2018). Dusk/dawn atmospheric asymmetries on tidally-locked satellites: O2 at europa. *Icarus*, *305*, 50–55. https://doi.org/10.1016/j.icarus.2017.12
Oza, A. V., Leblanc, F., Johnson, R. E., Schmidt, C., Leclercq, L., Cassidy, T. A., & Chaufray, J.-Y. (2019). Dusk over dawn o2 asymmetry in Europa's near-surface atmosphere. *Planetary and Space Science*, *167*, 23–32. https://doi.org/10.1016/j.pss.2019.01.006
Parisi, M., Caruso, A., Buccino, D. R., Gramigna, E., Withers, P., Gomez-Casajus, L., et al. (2023). Radio occultation measurements of Europa's ionosphere from Juno's close flyby. *Geophysical Research Letters*, *50*(22), e2023GL106637. https://doi.org/10.1029/2023GL106637
Paterson, W. R., Frank, L. A., & Ackerson, K. L. (1999). Galileo plasma observations at europa: Ion energy spectra and moments. *Journal of Geophysical Research*, *104*(A10), 22779–22791. https://doi.org/10.1029/1999JA900191
Plainaki, C., Milillo, A., Mura, A., Saur, J., Orsini, S., & Massetti, S. (2013). Exospheric o2 densities at europa during different orbital phases. *Planetary and Space Science*, *88*, 42–52. https://doi.org/10.1016/j.pss.2013.08.011
Richards, P. G., Fennelly, J. A., & Torr, D. G. (1994). Euvac: A solar euv flux model for aeronomic calculations. *Journal of Geophysical Research*, *99*(A5), 8981–8992. https://doi.org/10.1029/94JA00518
Richer, E., Modolo, R., Chanteur, G. M., Hess, S., & Leblanc, F. (2012). A global hybrid model for mercury's interaction with the solar wind: Case study of the dipole representation. *Journal of Geophysical Research*, *117*(A10). https://doi.org/10.1029/2012JA017898
Roth, L., Saur, J., Retherford, K. D., Strobel, D. F., Feldman, P. D., McGrath, M. A., & Nimmo, F. (2014). Transient water vapor at Europa's south pole. *Science*, *343*(6167), 171–174. https://doi.org/10.1126/science.1247051
Roth, L., Saur, J., Retherford, K. D., Strobel, D. F., Feldman, P. D., McGrath, M. A., et al. (2016). Europa's far ultraviolet oxygen aurora from a comprehensive set of hst observations. *Journal of Geophysical Research: Space Physics*, *121*(3), 2143–2170. https://doi.org/10.1002/2015JA022073
Rubin, M., Jia, X., Altwegg, K., Combi, M. R., Daldorff, L. K. S., Gombosi, T. I., et al. (2015). Self-consistent multifluid MHD simulations of Europa's exospheric interaction with Jupiter's magnetosphere. *Journal of Geophysical Research: Space Physics*, *120*(5), 3503–3524. https://doi.org/10.1002/2015JA021149
Saur, J., Strobel, D. F., & Neubauer, F. M. (1998). Interaction of the Jovian magnetosphere with Europa: Constraints on the neutral atmosphere. *Journal of Geophysical Research*, *103*(E9), 19947–19962. https://doi.org/10.1029/97JE03556
Schilling, N., Neubauer, F. M., & Saur, J. (2007). Time-varying interaction of Europa with the Jovian magnetosphere: Constraints on the conductivity of Europa's subsurface ocean. *Icarus*, *192*(1), 41–55. https://doi.org/10.1016/j.icarus.2007.06.024
Schilling, N., Neubauer, F. M., & Saur, J. (2008). Influence of the internally induced magnetic field on the plasma interaction of Europa. *Journal of Geophysical Research*, *113*(A3). https://doi.org/10.1029/2007JA012842
Schunk, R., & Nagy, A. (2009). *Ionospheres: Physics, plasma physics, and chemistry* (2nd ed.). Cambridge University Press. https://doi.org/10.1017/CBO9780511635342
Simon, S., Bößwetter, A., Bagdonat, T., Motschmann, U., & Glassmeier, K.-H. (2006). Plasma environment of Titan: A 3-d hybrid simulation study. *Annales Geophysicae*, *24*(3), 1113–1135. https://doi.org/10.5194/angeo-24-1113-2006
Sparks, W., Hand, K., McGrath, M., Bergeron, E., Cracraft, M., & Deustua, S. (2016). 09). Probing for evidence of plumes on Europa with hst/stis. *The Astrophysical Journal*, *829*(2), 121. https://doi.org/10.3847/0004-637X/829/2/121

21699402, 2025, 11, Downloaded from https://agupubs.onlinelibrary.wiley.com/doi/10.1029/2025JA033740 by Uppsala Universitet, Wiley Online Library on [04/12/2025]. See the Terms and Conditions (https://onlinelibrary.wiley.com/terms-and-conditions) on Wiley Online Library for rules of use; OA articles are governed by the applicable Creative Commons License

Szalay, J. R., Allegrini, F., Ebert, R., Bagenal, F., Bolton, S., Mccomas, D., & Wilson, R. (2024). Oxygen production from dissociation of Europa's water-ice surface. *Nature Astronomy*, *8*, 1–10. https://doi.org/10.1038/s41550-024-02206-x

Szalay, J. R., Smith, H. T., Zirnstein, E. J., McComas, D. J., Begley, L. J., Bagenal, F., et al. (2022). Water-group pickup ions from Europa-genic neutrals orbiting Jupiter. *Geophysical Research Letters*, *49*(9), e2022GL098111. https://doi.org/10.1029/2022GL098111

Wahlund, J.-E., Bergman, J. E. S., Åhlén, L. e. a., Puccio, W., Cecconi, B., Kasaba, Y., et al. (2025). The radio and plasma wave investigation (rpwi) for the Jupiter icy moons explorer (juice). *Space Science Reviews*, *221*(1), 1. https://doi.org/10.1007/s11214-024-01110-0

Werner, A. L. E., Leblanc, F., Chaufray, J. Y., Modolo, R., Aizawa, S., Hadid, L. Z., & Baskevitch, C. (2022). Modeling the impact of a strong x-class solar flare on the planetary ion composition in mercury's magnetosphere. *Geophysical Research Letters*, *49*(3), e2021GL096614. https://doi.org/10.1029/2021GL096614

Zimmer, C., Khurana, K. K., & Kivelson, M. G. (2000). Subsurface Oceans on europa and callisto: Constraints from Galileo magnetometer observations. *Icarus*, *147*(2), 329–347. https://doi.org/10.1006/icar.2000.6456

21699402, 2025, 11, Downloaded from https://agupubs.onlinelibrary.wiley.com/doi/10.1029/2025JA033740 by Uppsala Universitet, Wiley Online Library on [04/12/2025]. See the Terms and Conditions (https://onlinelibrary.wiley.com/terms-and-conditions) on Wiley Online Library for rules of use; OA articles are governed by the applicable Creative Commons License